Czech Technical University in Prague
Faculty of Electrical Engineering

Master thesis

Flight Control Laws and their Validation

Bc. Peter Mathia

supervised by
doc. Ing. Martin Hromčík, Ph.D.

May 26, 2017

CZECH TECHNICAL UNIVERSITY IN PRAGUE
Faculty of Electrical Engineering
Department of Measurement
Technická 2, 166 27 Prague 6, Czech Republic

Academic year **2016/2017**

MASTER PROJECT ASSIGNMENT

Student: **Bc. Peter Mathia**

Study programme: **Cybernetics and Robotics**
Specialisation: **Air and Space Systems**

Title of Master Project: **Flight Control Laws and their Validation**

Algoritmy řízení letu a jejich ověření (in Czech)

Guidelines:

The thesis objective is to demonstrate performance of selected advanced systems identification concepts and modern control design techniques in the context of flight controls, for selected flight mechanics models provided in the FlightGear simulator software. And perform validation and verification of selected results by means of computer simulation.

1. Implement interconnection between the FlightGear software and MATLAB Simulink and execute virtual data acquisition using selected simulation models.
2. Experiment with selected advanced systems identification techniques on the acquired data. Consider frequency-domain identification techniques and subspace identification methods.
3. Realize selected advanced flight control laws in MATLAB Simulink (MIMO LQR, dynamics inversion, etc.).
4. Validate selected results by high fidelity computer simulations.

Bibliography/Sources:

[1] Tischler Mark B., Remple Robert K.: Aircraft and Rotorcraft System Identification, Engineering Methods with Flight-test Examples, American Institute of Aeronautics and Astronautics, Restor, 2006

[2] Stevens Brian L., Lewis Frank L., Johnson Eric N.: Aircraft Control and Simulation, 3rd edition, Wiley 2016

Master Project Supervisor: doc. Ing. Martin Hromčík, Ph.D. (K 13135)

Valid until: September 30, 2018

ČESKÉ VYSOKÉ UČENÍ TECHNICKÉ V PRAZE Fakulta elektrotechnická -4- L.S.

Prof. Ing. Jan Holub, Ph.D.
Head of Department

Prof. Ing. Pavel Ripka, CSc.
Dean

Prague, February 1, 2017

Abstract [EN]

This thesis deals with fixed-wing aircraft dynamics model identification and flight-control system design using high fidelity aircraft simulator FlightGear.

First, the longitudinal and lateral linear state-space models are derived, which provide desired structure. The numeric values of these models are then identified using complex identification techniques based on frequency responses in CIFER® program, and compared with results obtained by MATLAB®/ Identification Toolbox®. The numeric vales are also computed from available FlightGear configuration and source files for verification of identification results.

Second, flight-control system is designed using modern, multi-input/multi-output (MIMO) techniques such as Linear Quadratic Regulator, and verified in the simulator test flight.

Keywords: aircraft, dynamics model, identification, control system, LQR, simulation

Abstrakt [SK]

Táto práca sa zaoberá identifikáciou dynamického modelu lietadla s pevným krídlom a návrhom riadiaceho systému s použitím letového simulátoru FlightGear.

Najprv je odvodený pozdĺžny a stranový lineárny stavový model lietadla, čo slúži ako základ a požadovaná štruktúra pre identifikáciu. Numerické hodnoty modelov sa následne určia pomocou komplexných techník založených na frekvenčných odozvách v programe CIFER® a v časovej oblasti v Identifikačnom Toolboxe MATLABu®. Číselné hodnoty sa takisto vypočítajú z dostupných konfiguračných a zdrojových súborov simulátoru FlightGear, čo slúži na overenie správnosti výsledkov.

Následne sa navrhne riadiaci systém s využitím moderných techník pre systémy s viacerými vstupmi a výstupmi, ako je LQR regulátor, a návrh sa overí pomocou testovacieho letu v simulátore.

Kľúčové slová: lietadlo, dynamický model, identifikácia, riadiaci systém, LQR, simulácia

Author's Affirmation

I hereby declare that the submitted thesis is exclusively my own work and that I have listed all used information sources in accordance with the Methodological Guideline on Ethical Principles for College Final Work Preparation.

2017 Prague author's signature

Acknowledgment

I would like to thank my thesis supervisor doc. Ing. Martin HROMČÍK, Ph.D. for letting me evaluate various design processes and methods used by aviation engineers today and for his valuable advices during the last year. He always was keen to help whenever I ran into a trouble or had a question about my thesis or writing and his door was always open for me when I needed it.

Contents

List of Figures

List of Tables

1 Introduction

"Modern planes can be flown by a pilot and a dog. Dog to bite the pilot if he touches the controls, and the pilot to feed the dog."

Aviation, and particularly, flight control design, has come a long way for this pilot's joke to be true. It all started in 1903 when Wright brothers successfully completed the first powered flight in history. However, their emphasis to make pilot control the airplane, instead of making it inherently stable, posed a huge difficulty in actually flying it. This quickly led to development of an automatic control system. In 1912 an autopilot was developed by the Sperry Gyroscope Company and tested on Curtiss flying boat.[3]

Skipping into 1970s, the invention of digital computer and flight control technology advances allowed the F-16 aircraft to be designed with relaxed static stability and controlled by state of the art fly-by-wire system.

In fact, most modern high performance jets, such as the already mentioned F-16, or Grumman/NASA X-29A forward-swept wing project shown bellow, couldn't even fly without modern sophisticated flight control systems. Moreover, this trend is now paving it's way from military into civil aviation, like for example the Boom® project, a 45 seat supersonic jet airliner, which should be the successor of Concorde, and which is already in testing phase.

This thesis presents an insight into design process of this modern control systems.

(a) Wright Flyer

(b) X-29A forward swept wing [1]

(c) Boom [2]

Figure 1: Aircraft evolution

[1]Image courtesy of Grumman/NASA
[2]Image courtesy of Boom Corporation

1.1 Classical control theory

Dynamics model is a foundation of every control system design. Classical control theory deals exclusively with single-input/single-output (SISO) systems or their parts. This allows only successive feedback loops closure, which leads to trial and error techniques of selecting individual gains and can be time consuming. On the other hand, this theory allows the system to be as simple as input-output description or transfer function, with no physical insights.

1.2 Modern control theory

In contrast, modern control theory deals with multi-input/multi-output (MIMO) systems and allows all the control gains of control system to be computed simultaneously, so that all loops are closed at the same time. Foundation of this approach is state-space dynamics model, which contains more information, such as physical insight into system, than simple SISO transfer function. Moreover, modern control theory allows the control systems to be designed faster and in a more direct and clean way than classical techniques.

1.3 Obtaining flight dynamics model

To be able to use modern control theory techniques, a state-space dynamics model is required. There are 2 techniques to obtain one:

1.) Simulation-based modeling, which involves adopting many a-priori assumptions about aircraft characteristics. The model is constructed from aerodynamic, inertial and structural characteristics of aircraft's individual parts, such as wings, tail, etc. The aerodynamic modeling can be based on principles such as finite-element theory, computational fluid dynamics (CFD) or empirical data. This physics-based modeling can be very labor intensive, time consuming, requiring the estimation or measurement of the aerodynamic, inertial, and structural properties of the many elements of the aircraft, but can be used before the aircraft is built.

2.) The second technique is system-identification modeling which is presented in more detail in Part II of this thesis.

1.4 Thesis goals

- perform test flights with selected high-performance aircraft using high-fidelity simulation software, for example FlightGear. During this flight, various maneuvers are executed to excite aircraft's dynamics modes and selected flight data, such as airspeed, Euler angles, angular velocities, etc are recorded.
- using test-flight data, perform system-identification to obtain aircraft's state-space model which is required for modern control algorithms. For the identification, non-traditional approaches are evaluated, such as frequency based methods explained by Tischler in [1] and exploited in CIFER® program, which are able to identify structured state-space models, and results compared with more traditional MATLAB®/Identification Toolbox®.
- design and implement control system for identified state-space model of selected aircraft using modern MIMO techniques. The most common MIMO controller is Linear Quadratic Regulator (LQR), which is described by Stevens in [3] and used in this thesis.
- validate implemented control system on non-linear model, for example during test flight in the simulation software.

Part I

Aircraft's linear model

2 Notations

The following notation is used thorough this thesis.

Aerodynamic forces:
- L - lift
- D - drag
- C - cross-wind force

Euler angles:
- ϕ - roll
- θ - pitch
- ψ - yaw

Control surface deflections:
- *el* - elevator
- *thr* - thrust
- *ail* - aileron
- *rud* - rudder

Angular velocities:
- p - roll rate
- q - pitch rate
- r - yaw rate

Aerodynamic angles:
- β - side-slip angle
- α - angle of attack

Airspeed in equilibrium: V_e

3 Linear state-space model

Modern MIMO flight control system design methods, such as LQR used in the thesis, are based on state-space theory and require an accurate state-space model.

The state-space model structure is traditionally derived from non-linear equations of motion in a selected steady-state point - equilibrium, and is valid for small perturbations from this point. The unknown parameters can be stability and control derivatives of the classical flight mechanics equations, or physical constants, e.g. gravity.

3.1 Equilibrium and steady-state flight

Implicit state equations are of the form

$$\mathbf{f}(\dot{\mathbf{X}}, \mathbf{X}, \mathbf{U}) = \mathbf{0} \tag{3.1}$$

where $\mathbf{f}$ is an array of n non-linear functions f_i, $\mathbf{X}$ is a state vector, $\mathbf{U}$ is input vector. [3]

The coordinates of a singular point of the implicit non-linear state equations are given by a solution, $\mathbf{X} = \mathbf{X}_e$, which satisfies

$$\mathbf{f}(\dot{\mathbf{X}}, \mathbf{X}, \mathbf{U}) = \mathbf{0}, \text{ with } \dot{\mathbf{X}} \equiv \mathbf{0};\ \mathbf{U} \equiv \mathbf{0} \text{ or constant} \tag{3.2}$$

Steady-state aircraft flight can be defined as a "condition in which all of the force and moment components in the body-fixed coordinate system are constant or zero." [3]

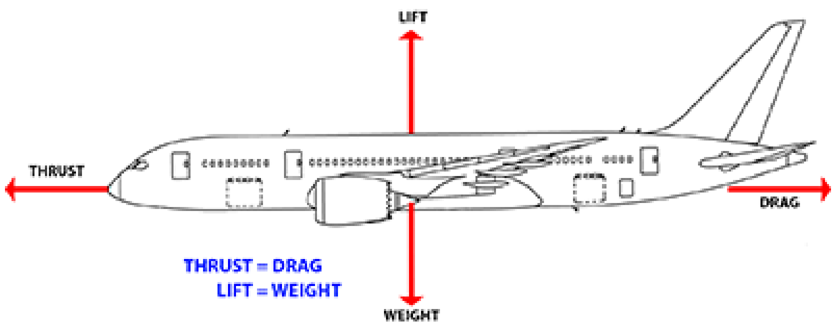

Figure 2: Steady-state flight

3.2 Model structure

Since the process of deriving linear state-space model from non-linear equations is out of scope of this thesis, the model is used as given in [1] and [3].

The perturbation equations of motion of a MIMO linear-time-invariant (LTI) system are composed of n states $x_1, x_2, \dots, x_n$ and n_c control inputs $u_1, u_2, \dots, u_n$ and can be written in matrix form

$$\mathbf{M}\dot{\mathbf{x}} = \mathbf{F}\mathbf{x} + \mathbf{G}\mathbf{u} \tag{3.3a}$$

$$\mathbf{y} = \mathbf{H_0}\mathbf{x} + \mathbf{H_1}\dot{\mathbf{x}} \tag{3.3b}$$

where matrices $\mathbf{M}, \mathbf{F}, \mathbf{G}, \mathbf{H_0}, \mathbf{H_1}$ contain the unknown stability and control derivatives of the classical flight-mechanics equations, or physical constants.

State-space model of a typical aircraft can be separated into longitudinal and lateral parts, which can be later treated separately. This significantly reduces complexity of both identification process and control systems design.

3.3 Longitudinal model

State vector

$$\mathbf{x} = \begin{bmatrix} \alpha & q & v & \theta \end{bmatrix}^T \tag{3.4}$$

Control vector

$$\mathbf{u} = \begin{bmatrix} el & thr \end{bmatrix}^T \tag{3.5}$$

State matrices

$$\mathbf{M} = \begin{bmatrix} V_e - Z_{\dot{\alpha}} & 0 & 0 & 0 \\ -M_{\dot{\alpha}} & 1 & 0 & 0 \\ 0 & 0 & 1 & 0 \\ 0 & 0 & 0 & 1 \end{bmatrix}, \quad \mathbf{G} = \begin{bmatrix} Z_{el} & -X_{thr}\sin(\alpha_e + \alpha_T) \\ M_{el} & M_{thr} \\ X_{el} & X_{thr}\cos(\alpha_e + \alpha_T) \\ 0 & 0 \end{bmatrix}$$

$$\mathbf{F} = \begin{bmatrix} Z_\alpha & V_e + Z_q & Z_V - X_{T_V}\sin(\alpha_e + \alpha_T) & -g_D \sin\gamma_e \\ M_\alpha + M_{T_\alpha} & M_q & M_V + M_{T_V} & 0 \\ X_\alpha & 0 & X_V + X_{T_V}\cos(\alpha_e + \alpha_T) & -g_D\cos\gamma_e \\ 0 & 1 & 0 & 0 \end{bmatrix}, \quad \mathbf{H_0} = \mathbf{I_4}, \quad \mathbf{H_1} = \mathbf{0}$$

3.3.1 Modes

Dynamic modes of state-space model can be analyzed from position of it's poles.

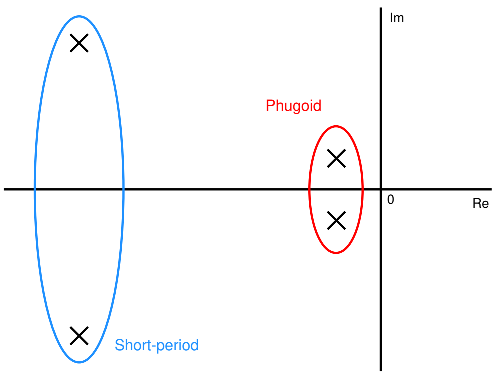

Figure 3: Typical poles position of longitudinal aircraft model

Short-period

The short-period is dominated by changes in angle of attack α and pitch-rate q. [4]

Phugoid

The phugoid mode is dominated by large changes in velocity and corresponds to cyclic trade-offs in kinetic energy (velocity) and potential energy (height). [4]

3.4 Lateral model

State vector

$$\mathbf{x} = \begin{bmatrix} \beta & \phi & p & r \end{bmatrix}^T \tag{3.6}$$

Control vector

$$\mathbf{u} = \begin{bmatrix} ail & rud \end{bmatrix}^T \tag{3.7}$$

State matrices

$$\mathbf{M} = \begin{bmatrix} V_e & 0 & 0 & 0 \\ 0 & 1 & 0 & 0 \\ 0 & 0 & 1 & 0 \\ 0 & 0 & 0 & 1 \end{bmatrix}, \qquad \mathbf{G} = \begin{bmatrix} Y_{ail} & Y_{rud} \\ 0 & 0 \\ L_{ail} & L_{rud} \\ N_{ail} & N_{rud} \end{bmatrix}$$

$$\mathbf{F} = \begin{bmatrix} Y_\beta & g_D \cos\theta_e & Y_p & Y_r - V_e \\ 0 & 0 & \cos\gamma_e / \cos\theta_e & \sin\gamma_e / \cos\theta_e \\ L_\beta & 0 & L_p & L_r \\ N_\beta & 0 & N_p & N_r \end{bmatrix}, \quad \mathbf{H_0} = \mathbf{I_4}, \quad \mathbf{H_1} = \mathbf{0}$$

3.4.1 Modes

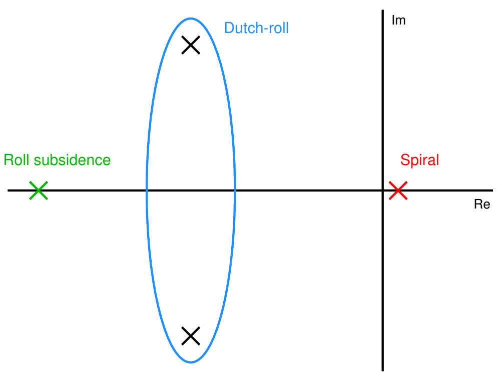

Figure 4: Typical poles position of lateral aircraft model

Roll subsidence

The roll-rate p is dominant in the roll subsidence. It is almost purely motion about the body x-axis. This mode is the fastest of lateral-directional modes. [4]

Dutch-roll

The Dutch-roll is dominated by the variables β and r. It is slower than the roll subsidence but faster than the spiral. [4]

Spiral

The spiral mode has dominance in bank-angle ϕ. Unlike the roll subsidence, however, there is no accompanying large roll-rate. If this eigenvalue had been positive then the interpretation would have been of slowly increasing bank angle. [4]

Part II

System identification

4 System identification

According to Tischler [1], system identification is a highly versatile procedure for rapidly and efficiently extracting accurate dynamic models from the measured response to specific control inputs. Models might characterize the dynamics as a whole or a subsystem, such as an actuator, rotor system, or the engine.

An aircraft can be considered as an input-output system. The dynamics are excited by the control inputs, which in the current case are the conventional aerodynamic surfaces: aileron *ail* for roll control, elevator *el* for pitch control, rudder *rud* for yaw control and throttle *thr* for speed control. Output signals as an aircraft dynamic response, are then measured during excitation and recorded into time-history database for further analysis. In this case, excitation and output signals recording are performed in FlightGear simulator.

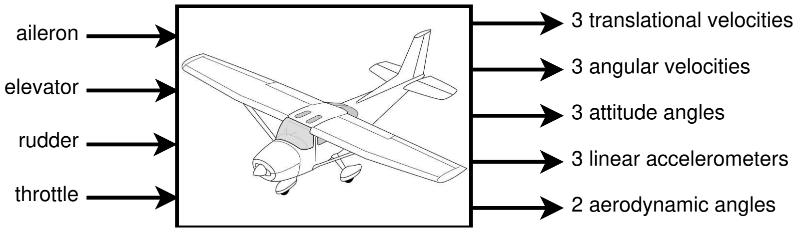

Figure 5: Aircraft as an input-output system [1]

A dynamic model relates the control inputs to the aircraft dynamic response. This model can be as complex as a set of differential equations of motion. Dynamic models are needed for many applications, including analysis of aircraft stability and control, piloted simulations, flight control design, and analysis of aircraft handling characteristics.

4.1 Simulation vs system identification

System identification and simulation modeling can be seen as inverse procedures. In system modeling, aircraft behavior is characterized by differential equations of motions, which are built up from mathematical modeling of individual aircraft's parts, such as wings, fuselage, tail etc. This method uses principles such as finite element methods or empirical aerodynamics and structural data. On the other hand, in system identification, the aircraft response is measured, and a dynamic model is extracted from the data, the reverse of developing a simulation.

Key applications of system identification results include piloted simulation models, comparison of wind-tunnel vs flight measurements, validation and improvements of physics-based simulation models and flight control system development.

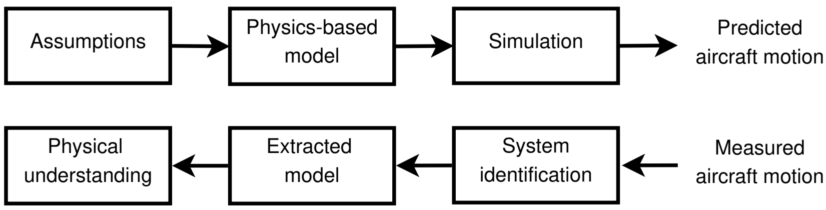

Figure 6: Simulation vs identification [1]

4.2 Frequency response identification method

There are many methods used for system identification, which produce satisfactory results, but methods developed by Tischler[1] using frequency responses are well suited for aircraft flight data, and will be evaluated and tested in this thesis. The results will be compared with MATLAB®/Identification Toolbox® , which works in time domain.

Differences between the frequency response and time response methods as cited by Tischler [1]:

Characteristic	Frequency-response methods	Time-response methods
Initial data	consist of frequency responses (derived from time-history data)	consist of time-history data
How models are identified	by matching predicted frequency responses against measured frequency responses	by matching predicted time histories against measured time histories
Noise	bias effects of noise in response measurements and process noise are eliminated from the analysis	noise models must be identified; if noise is ignored, biases will be introduced in identification results
Independent measure provided	coherence function provides a direct and independent measure of system excitation, data quality and system response linearity	no independent metric to access system excitation and linearity
Responses	response pairs are fit only in the frequency range over which the data is accurate	fit over the same time and frequency ranges
Time delays	direct and precise identification	not identified directly
Bias or reference shifts	no biases or reference shifts to be identified	must be identified and can be correlated with aerodynamic parameters
Number of points	small number of points are included in iterative criterion	large number of points (time-history data)
Algorithms or equations used	very efficient because frequency responses are determined algebraically from updated parameters	equations of motions must be numerically intergated in time for each iterative update
Unstable systems	good results	special techniques used can degrade the quality of results

Table 1: Frequency methods vs time methods [1] p.16

4.3 CIFER® software

CIFER® - Comprehensive Identification from FrEquency Responses, is a software which uses frequency response based identification techniques. It has been developed by Tischler[1] and its possibilities are evaluated in this thesis.

Figure 7: CIFER® software [1]

The foundation of the CIFER® software approach is the high-quality extraction of a complete multi-input/multi-output (MIMO) set of non-parametric input-to-output frequency responses. These responses fully characterize the coupled characteristics of the system without a-priori assumptions.[1]

Advanced Chirp-Z transform and composite optimal window techniques developed and exercised with over 25 years of flight project applications provide significant improvement in frequency-response quality relative to standard Fast Fourier Transforms (FFTs). Sophisticated non-linear search algorithms are used to extract a state-space model which matches the complete input/output frequency response data set.[1]

4.3.1 Key features

- identification algorithms that have been extensively applied and proven on many flight projects
- implementation of frequency-response identification in a step-by-step sequence of core programs
- multi-input frequency response solution
- highly flexible and interactive definition of identification model structures
- fully automated weighting-function selection based on frequency response accuracy
- reliable parameter accuracy metrics
- integrated procedure for identification and model structure determination
- time-domain verification of models, including identification of offsets and biases
- integrated and efficient databasing of all results

5 Collection of time-history data

Key part of identification process is time-history data collection. In practice, this is done by performing test flights using real aircrafts, where required measurements, e.g. control surface deflections, attitude angles, airspeed, angle of attack etc., are logged into database. In this case, since a real aircraft is not available, an open-source flight simulator, FlightGear, is used.

5.1 MATLAB® -FlightGear interface

5.1.1 FlightGear

FlightGear is an open-source flight simulator. It supports a variety of popular platforms (Windows, Mac, Linux, etc.) and is developed by volunteers from around the world. Source code for the entire project is available and licensed under the GNU General Public License.

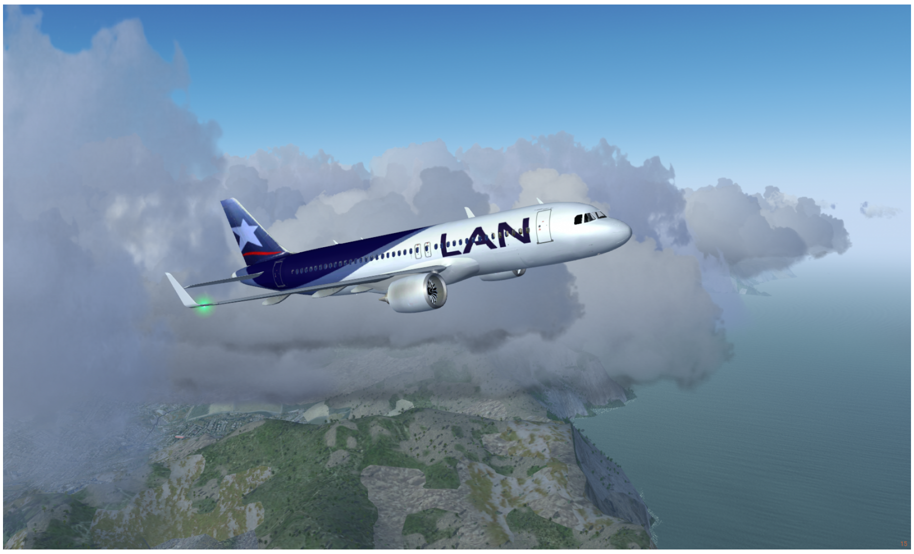

Figure 8: FlightGear flight simulator

"The goal of the FlightGear project is to create a sophisticated and open flight simulator framework for use in research or academic environments, pilot training, as an industry engineering tool and as a fun, realistic, and challenging desktop flight simulator."

One of the most important features which is essential in aircraft dynamics identification and control are fully exposed internal properties. That means, FlightGear allows users and aircraft designers access to a very large number of internal state variables via numerous access mechanisms. These state variables are organized into a convenient hierarchal property-tree. Using the property-tree, it is possible to monitor just about any internal state variable. It's possible, for example, to remotely control FlightGear from an external script, or to create model animations, sound effects, instrument animations and network protocols for about any situation imaginable just by editing a small number of human readable configuration files.

This is a powerful system that makes FlightGear immensely flexible, configurable, and adaptable.

5.1.2 Interface implementation

The easiest approach how to externally control aircraft model in FlightGear is via UDP protocol. The required properties that need to be accessed are defined in the already mentioned property-tree. The interface can be defined in an XML file, as shown bellow:

```
<?xml version="1.0"?>
<PropertyList>
    <generic>
        <input>
            <line_separator>newline</line_separator>
            <var_separator>tab</var_separator>
            <chunk>
                <name>/controls/flight/elevator</name>
                <node>/controls/flight/elevator</node>
                <type>float</type>
                <format>%.4f</format>
            </chunk>
        </input>
    </generic>
</PropertyList>
```

After creating XML files for both input (elevator, throttle) and output properties (airspeed, pitch angle...) and storing them in FlightGear protocols folder, FlightGear is started via command line with following command:

```
fgfs --generic=socket,out,40,localhost,5502,udp,output_con
```

The number 40 is sampling frequency at which UDP packets will be sent to and from FlightGear. More about sampling frequency is in section 5.5. 5502 is a number of port to which UDP packets will be send to.

The last thing to do is to create functions in MATLAB®/Simulink® to send and receive UDP packets.

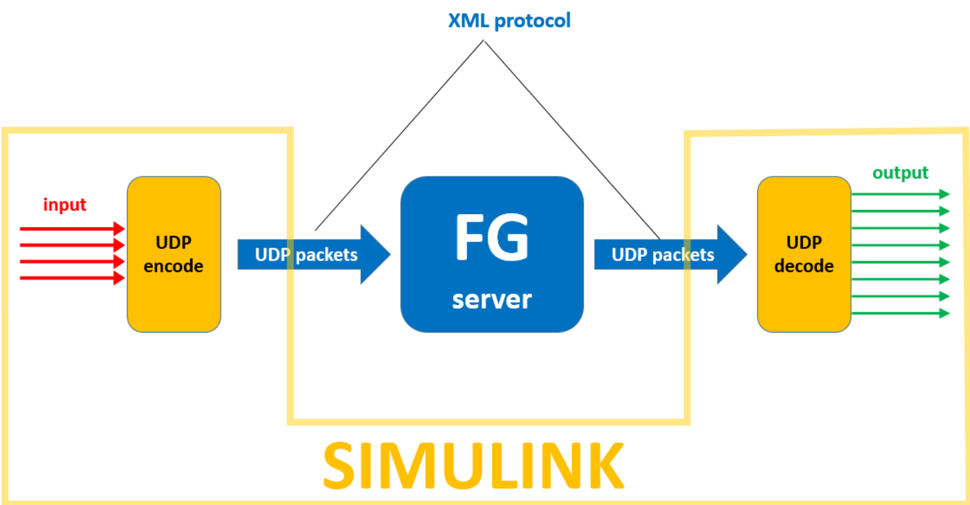

Figure 9: Flight gear MATLAB®/Simulink® interface

The picture above shows the interface. The result is an airplane model that can be controlled from MATLAB®/Simulink® in real-time.

5.2 Selected aircraft

For the purposes of this thesis, an icon in aviation industry has been selected - Concorde.

Concorde was a supersonic civil aircraft operated by British Airways and Air France. The main reason why it was selected was one of the highest rating in FlightGear aircrafts available for download and also because it is a high performance aircraft with typical dynamics characteristics, unlike many fighter jets which have unstable static stability.

Figure 10: Concorde

5.2.1 Technical details

Length	61.66m
Wingspan	25.60m
Height	12.20m
Wing area	358.25m^2
Empty weight	78,700kg
Max takeoff weight	185,000kg
Powerplant	4 × Rolls-Royce/SNECMA, Olympus 593 Mark 610 turbojet
Cruise speed	Mach 2.04
Max operating altitude	60,000ft

Table 2: Concorde technical details

5.3 Desired frequency range

Before starting the identification process, it is desired to define the frequency range of applicability for the model.

Each modeling result of system identification (i.e., a frequency response, a transfer-function model, or a state-space model) has associated with it a frequency range of applicability, defined as "frequency range over which the identified model can be expected to be valid." [1]

The required frequency range of applicability is determined by intended application of the system identification model, i.e. handling qualities validation, control system design, structural modes. Since the thesis deals with control system design, the range of $[\omega_{min}, \omega_{max}] = [0.03; 10]$ rad/s is selected.

5.4 Recommended excitation inputs

The excitation signals for system identification must be designed to suitably excite the aircraft modes that are to be modeled. The best suited type of signal is frequency-sweep.

5.4.1 Frequency sweep

A class of control inputs that has a quasi-sinusoidal shape of increasing frequency. The frequency-sweep input is, according to Tischler[1], particularly well suited for the frequency response method for a number of reasons:

1. The power spectral density (PSD) has a very uniform distribution across the desired frequency range. That means all dynamics modes are satisfactorily excited in the desired frequency range and consistent level of frequency response coherence (accuracy) is achieved.

2. Response time-histories are roughly symmetric. This means that the deviations in inputs are generally equal around the equilibrium (trim) point. This symmetry is important both for maintaining the flight centered around the trim condition and for determining and subtracting out the trim value of the input and output signals in the subsequent Fourier analysis.

3. The frequency range of excitation is strictly controlled during the test. The frequency sweep test starts at a predefined minimum frequency and ends at a predefined maximum frequency. Both frequencies are easily monitored in real time. Controlling the frequency range of the test in this way can be quite important aspect of the safety of flight-test procedure (i.e avoid flutter and structural damage at high frequencies)

5.4.2 Sweep construction

The record starts and ends with the aircraft in a trim state (3s). Record of the trim condition is important for the spectral analysis, which subtracts the trim state from the data.

The next point is that the sweep starts with two low frequency input cycles and then progresses smoothly to the mid and higher frequencies. The low frequency input is not a pure sine wave, and so this part of the sweep actually ensures good identification over a range of frequencies around ω_{min}.

$$f_{min} = \frac{\omega_{min}}{2\pi} \tag{5.1}$$

$$f_{max} = \frac{\omega_{max}}{2\pi} \tag{5.2}$$

$$T_{min} = \frac{1}{f_{max}} \tag{5.3}$$

$$T_{max} = \frac{1}{f_{min}} \tag{5.4}$$

Guideline [1]:

$$T_{rec} \geq (4 \text{ to } 5)T_{max} \tag{5.5}$$

Thus, about 40% of the sweep is associated with the two low frequency inputs (at ω_{min}). The remaining time is used to complete the buildup to the maximum frequency ω_{max} and to establish trim at the start and end of the record.

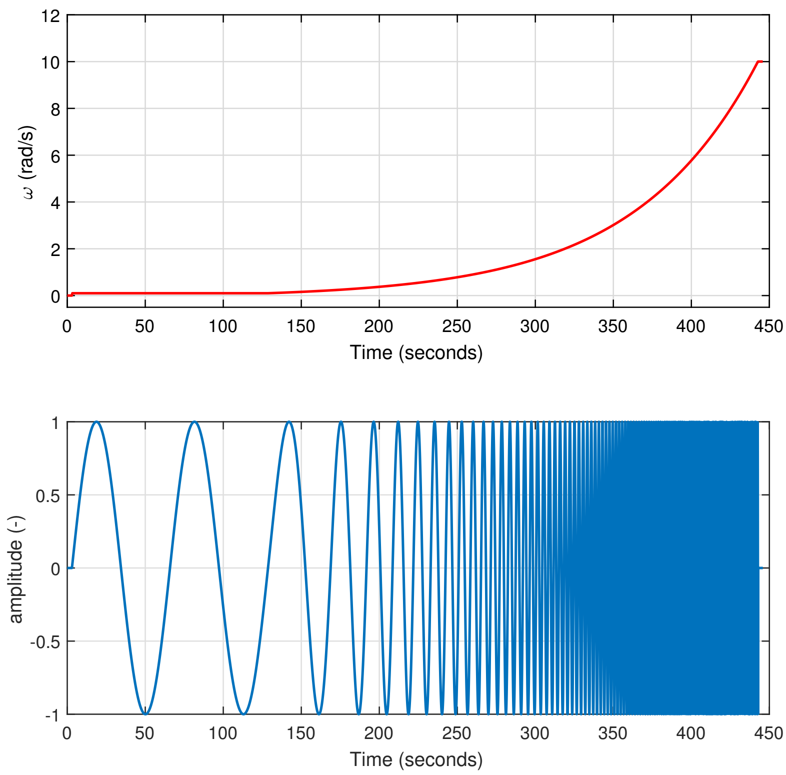

Figure 11: Frequency sweep signal

The magnitude of the sweep input is typically in the range of $\pm 10 - 20\%$ of control inputs and does not have to be exactly symmetric or constant.

Multiple flight records are concatenated into a single one. This ensures a rich spectral content.

5.4.3 Computer-generated sweep

Due to lack of piloting skills, computer-generated sweep is used in this case, with manual impulses when needed to keep the flight around trim conditions.

However, it must be properly synthesized in order to obtain the desired frequency spectrum.

Computer generated excitation signal uses an exponential sweep and white noise. The exponentially increasing sweep frequency is used to ensure that more time is spent at the lower frequencies (longer characteristic periods) and less time at the higher frequencies (shorter characteristic periods).

The frequency-sweep component is generated by the equation

$$\delta_{sweep} = A \sin[\theta(t)] \tag{5.6}$$

where A is the sweep amplitude, typically 10% of the maximum deflection limits, and

$$\theta(t) = \int_0^{T_{rec}} \omega(t)\ \mathrm{d}t \tag{5.7}$$

The frequency progression is given by

$$\omega = \omega_{min} + K(\omega_{max} - \omega_{min}) \tag{5.8}$$

where

$$K = C_2 \left[exp\left(\frac{C_1\ t}{T_{rec}} \right) - 1 \right] \tag{5.9}$$

The values $C_1 = 4.0$ and $C_2 = 0.0187$ have, according to Tischler [1], been found to be suitable for a wide range of applications.

Computer-generated sine sweeps alone might sometimes not constitute an excitation signal with sufficient spectral richness because they will not have any of the irregularities in input shape that are evident in a pilot-generated sweep. So, if necessary, a band-limited white-noise component can be added to the sweep to enrich the spectral content:

$$\delta_{excitation} = \delta_{sweep} + \delta_{white-noise} \tag{5.10}$$

A typical rms (1σ) level of the noise signals is selected as

$$\delta_{white-noise} :\ \sigma = 0.10A \tag{5.11}$$

5.5 Sample rate and filters

The selection of the appropriate data collection sample rate and data system filters flows directly from the frequency range of applicability of the identified model.

The white-noise component of collected signals should be processed with a low-pass filter ω_f to suppress high frequency content in the excitation.

Guideline [1]:

- filter cut-off frequency

$$\omega_f = 5 \cdot \omega_{max} \tag{5.12}$$

- sample rate

$$\omega_s = 5 \cdot \omega_f \tag{5.13}$$

6 Data consistency

6.1 Modeling measurements errors in flight-test data

Since the ideal, noise-free measurement doesn't exist in real world, there might be multiple errors in the obtained flight data.

Measurement errors are broadly classified as deterministic (systematic) or non-deterministic (random). Common sources of deterministic errors include bias, scale factor and drift.

6.2 Kinematic consistency

For example, consider the measurement of Euler roll angle ϕ. In most cases, the flight measurement ϕ_m can be expressed in terms of the estimated (i.e., corrected) value ϕ_e by the parametric equation

$$\phi_m(t-\tau_\phi) = \lambda_\phi \phi_e(t) + b_\phi + n_\phi \tag{6.1}$$

where the error parameters are: $\tau_\phi \equiv$ time shift, $\lambda_\phi \equiv$ scale factor, and $b_\phi \equiv$ bias to account for the deterministic errors. The last parameter, $n_\phi \equiv$ noise, is generally modeled as zero-mean white-noise and encompasses random errors.[1]

6.2.1 Angular consistency

Linearized Euler relationships:

$$p = \dot{\phi} \tag{6.2}$$

$$q = \dot{\theta} \tag{6.3}$$

$$r = \dot{\psi} \tag{6.4}$$

Laplace transform:

$$p = s\phi \tag{6.5}$$

$$q = s\theta \tag{6.6}$$

$$r = s\psi \tag{6.7}$$

Roll-angle measurement:

$$\phi_m(t) = \lambda_\phi \phi(t) \tag{6.8}$$

Roll-rate measurement:

$$p_m(t) = \lambda_p p(t) \tag{6.9}$$

Frequency response:

$$\frac{p_m}{\phi_m}(s) = Kse^{-\tau s} \tag{6.10}$$

where the constant K is the ratio of scale factors,

$$K = \frac{\lambda_p}{\lambda_\phi} \tag{6.11}$$

and any relative time shift in the data caused by filtering or skewing will be absorbed in τ, the effective time delay. The values of K and τ are determined from a transfer-function fit of the frequency response p_m/ϕ_m.[1]

7 SISO Frequency response identification

"The analysis of a signal or input-to-output process as a function of frequency (rather than time) is referred to as spectral analysis." [1]

7.1 Definition of frequency response

The Fourier transform takes non-periodic time-based input and output signals $x(t)$ and $y(t)$, respectively, and transforms them into two equivalent frequency based signals $X(f)$ and $Y(f)$, where

$$X(f) = \int_{-\infty}^{\infty} x(t) e^{-j2\pi f t} \mathrm{d}t \tag{7.1}$$

and

$$Y(f) = \int_{-\infty}^{\infty} y(t) e^{-j2\pi f t} \mathrm{d}t \tag{7.2}$$

are referred to as the Fourier coefficients.

Frequency response $H(f)$ is now the complex-valued function that relates Fourier coefficients of the input $X(f)$ and output $Y(f)$ by means of the equation

$$Y(f) = H(f)X(f) \tag{7.3}$$

The frequency-response function $H(f)$ is just the ratio of the output to the input transforms.

$$H(f) = \frac{Y(f)}{X(f)} = H_R(f) + jH_I(f) \tag{7.4}$$

$$\text{Magnification factor} = |H(f)| = \sqrt{H_R^2(f) + H_I^2(f)} \tag{7.5}$$

$$\text{Phase shift} = \varphi(f) = \angle H(f) = \arctan\left[\frac{H_I(f)}{H_R(f)}\right] \tag{7.6}$$

The frequency response $H(f)$ fully characterizes the system's dynamic behavior, in terms of the best linear description of the input-to-output behavior, without imposing a requirement for any a-priori knowledge about the internal structure of the system's equations of motion. [1]

7.2 Frequency response interpretation

A convenient graphical visualization of the frequency response function is a Bode plot, which is a semi-log plot of the magnitude of H in decibels (H_{dB}) and the phase of H in degrees (H_{deg}), both vs frequency, usually in rad/s. The vertical axis (dB, deg) uses linear scale, and the horizontal axis (frequency) uses a log scale.

$$H_{dB} = 20\ \log_{10}|H(j\omega)| \tag{7.7}$$

$$H_{deg} = \angle H(j\omega)\ deg \tag{7.8}$$

7.3 Fourier transform and spectral functions in practice

7.3.1 Discrete Fourier transform

The discrete Fourier transform (DFT) determines $X(f)$ at discrete frequencies f_k from a finite record of sampled data:

$$X(f_k) = X(k\Delta f) = \Delta t \sum_{n=0}^{N-1} x_n \cdot exp\left[\frac{-j2\pi(kn)}{n}\right] \tag{7.9}$$

where

$$\begin{aligned} X(f_k) &= \text{Fourier coefficients, for } k = 0,1,2,...,N-1 \\ x_n = x(n\Delta t) &= \text{time} - \text{domain data record, for } n = 0,1,2,...,N-1 \\ \Delta t &= \text{time increment} \\ \Delta f = 1/N\Delta t &= \text{frequency resolution} \\ N &= \text{number of discrete frequency points} \end{aligned}$$

The number of discrete frequency points in the identified Fourier transform $X(f_k)$ is the same as the number of discrete time points in the time-history data record x_n, namely N. The frequency points are distributed evenly from $f_{min} = \Delta f$ to the sample rate $(f_s = 1/\Delta t)$.
$\Rightarrow$ bad resolution within the required frequency range $\Rightarrow$ use chirp-z transform

7.3.2 Fast Fourier and chirp-z transform

Frequency response determination using Discrete Fourier transform is computationally intensive. The Fast Fourier transform (FFT) is a numerically more efficient algorithm.

A specialized implementation of the FFT is the chirp-z transform (CZT), also known as the zoom transform. The CZT is capable of a highly accurate frequency response determination.

Key properties of the CZT vs FFT [1]:

1. The number of frequency points N is specified independently of the number of time-history points L. This relaxes the rather severe FFT restriction that $N = L$.

2. The N frequency points of the CZT are distributed over an arbitrary arc of the unit circle (i.e., only in the frequency range of interest), not over the frequency range of the entire unit circle as in the case of the FFT. This increases the frequency resolution in the range of interest (i.e. frequency range of interest is between ω_{min} and ω_{max}, not up to $f_s/2$)

3. The CZT is subject to reduced leakage, or digital contamination, and it has improved accuracy as compared to the FFT.

7.3.3 Spectral functions

The products of the Fourier transform computation are the Fourier coefficients of the input (excitation) $X(f)$ and output (response) $Y(f)$. From these, three important spectral functions are defined by Tischler [1]:

1. Input auto-spectrum
$$\tilde{G}_{xx}(f) = \frac{2}{T}|X(f)|^2 \tag{7.10}$$

The input auto-spectrum, also referred to as the input power spectral density (PSD), displays the distribution of the squared input x^2 or excitation power as a function of frequency f.

2. Output auto-spectrum
$$\tilde{G}_{yy}(f) = \frac{2}{T}|Y(f)|^2 \tag{7.11}$$
A rough estimate of output auto-spectrum, or PSD, displays the distribution of the squared output y^2 or response power as a function of frequency.

3. Cross-spectrum
$$\tilde{G}_{xy}(f) = \frac{2}{T}[X^*(f)Y(f)] \tag{7.12}$$
The cross-spectrum displays the distribution of the product of input times output xy or input-to-output power transfer as a function of frequency.

where * denotes the complex conjugate value, and $\tilde{G}$ denotes a rough estimate. $T = T_{rec}$ denotes a single flight record length.

7.3.4 Interpreting spectral functions

A direct application of the spectral functions is in the evaluation of excitation and aircraft response frequency content for a system identification maneuver. Sudden descent in the input auto-spectrum indicates that the pilot input might have passed through that frequency too quickly, and maneuver has to be repeated.

7.3.5 Frequency response calculation

The frequency response function $H(f)$ can be estimated directly from the smooth spectral function estimates at each frequency point f.

$$\hat{H}(f) = \frac{\hat{G}_{xy}(f)}{\hat{G}_{xx}(f)} = \frac{\hat{G}_{yy}(f)}{\hat{G}_{yx}(f)} \tag{7.13}$$

7.3.6 Coherence function

Another important product of the smooth spectral functions is the coherence function estimate $\hat{\gamma}^2_{xy}$, defined at each frequency f by

$$\hat{\gamma}^2_{xy}(f) = \frac{\left|\hat{G}^2_{xy}(f)\right|^2}{\left|\hat{G}xx(f)\right|\left|\hat{G}yy(f)\right|} \tag{7.14}$$

The coherence function can be interpreted physically as the fraction of the output spectrum G_{yy} that is linearly attributable to the input spectrum G_{xx} at frequency f. The values of coherence function range between 0 and 1.

Following some basic rule of thumb, the coherence function can be used to effectively and rapidly assess the accuracy of the frequency response identification. Generally speaking, as long as the coherence function satisfies the condition

$$\gamma^2_{xy} \geq 0.6 \tag{7.15}$$

and is not oscillating, the frequency response will have acceptable accuracy. [1]

7.4 Windowing

Random errors in the spectral function calculations can be greatly reduced using windowing methods. The method of overlapped windowing, also called the method of periodograms, is a key technique in practical spectral analysis that greatly reduces the level of random error in the spectral estimates. This technique produces smooth spectral estimates by averaging the rough estimates for multiple segments of data. [1]

The original time-history record (duration T_{rec}) is segmented into a sequence of n_r shorter overlapping time segments or windows of length T_{win}, each window containing L points. The time-history for the last window is filled out to its completion by appending the trim value to the time history beyond the flight record duration. [1]

The time-history data in each window segment are weighted by the window shaping function $w(t)$ to form the weighted time-history segment. This window tapering reduces the spectral errors associated with side-lobe leakage that is characteristic of strict rectangular windowing. [1]

The window width T_{win} determines directly the minimum frequency f_{min} and frequency resolution Δf of the DFT:

$$f_{min} = \Delta f = \frac{1}{T_{win}} = \frac{1}{L\Delta t} = \frac{f_s}{L} \tag{7.16}$$

$$f_{max} = \frac{f_s}{5} \tag{7.17}$$

7.4.1 Window size selection

Guideline	Topic
$n_d \geq 5$	Number of independent windows based on combination of record length and window length
$T_{win} = 2T_{max}$	Nominal window size T_{win} relative to the length of the longest period of interest T_{max}
$T_{win} \leq 0.5T_{rec}$	Maximum window size T_{win} relative to the length of the record T_{rec}
$T_{win} \leq (1/5)T_F$	Maximum window size T_{win} relative to the concatenated record length $T_F = 3 \cdot T_{rec}$
$T_{win} \geq 20(2\pi/\omega_{max})$	Minimum window size T_{win} relative to the maximum frequency of interest

Table 3: Window selection guidelines [1]

7.4.2 Composite windowing

Large window lengths produce good coherence (accuracy) results at lower frequencies, and small window lengths at higher frequencies.

Composite windowing is a procedure, that merges frequency response results obtained for different window lengths into one frequency response, with acceptable coherence throughout the whole frequency range of interest.

More details about this procedure can can be found in Tischler [1].

8 Transfer-function identification

Transfer function models, that accurately match the flight-data frequency responses and characterize the overall input-to-output response dynamics can be identified. They are most commonly used to represent the SISO on-axis response of the flight vehicle (e.g. q/el) or subsystem. [1]

The system to be modeled is treated like a black box without any insight into actual physics of the aircraft using force and moment equations and the associated physical constraints (e.g. gravity and kinematics). Instead, transfer-function models are composed of a numerator and denominator polynomial in the Laplace variable s.

A transfer-function model of the generalized form

$$H(s) = \frac{(b_0 s^m + b_1 s^{m-1} + \cdots + b_m)e^{-\tau_{eq}s}}{(s^n + a_1 s^{n-1} + \cdots + a_n)} \tag{8.1}$$

is found that best matches the identification frequency response data, where

$$m \leq n \tag{8.2}$$

The orders of the numerator m and denominator n are chosen in identification process to achieve a good fit of the frequency response data in the frequency range of interest.

In the transfer-function identification process, each of the coefficients a_i and b_i of the polynomials and equivalent time delay τ_{eq} can be individually fixed or freed (in the latter case, to be optimized).

A numerical optimization algorithm determines the set of unknown (i.e. freed) quantities in equation (8.1) that minimizes the magnitude and phase errors between the desired SISO transfer-function model H and the associated composite frequency response estimate (i.e. data) $\hat{H}_c$. [1]

8.1 Cost function

The quadratic cost function J, suggested by Tischler[1], to be minimized is

$$J = \frac{20}{n_\omega} \sum_{\omega_1}^{\omega_{n_\omega}} W_\gamma \left[W_g(|\hat{H}_c| - |H|)^2 + W_p(\angle \hat{H}_c - \angle H)^2 \right] \tag{8.3}$$

where

$$\begin{aligned} |\;| &= \text{magnitude (dB) at each frequency } \omega \\ \angle &= \text{phase (deg) at each frequency } \omega \\ n_\omega &= \text{number of frequency points} \\ \omega_1 \text{ and } \omega_{n_\omega} &= \text{starting and ending frequencies of fit} \end{aligned}$$

By selecting the n_ω frequency points in a uniform spacing over a log-frequency scale (rad/s), the minimization achieves a best fit on the Bode plot.

The other parameters of cost function are as follows:

1. W_γ is a weighting function dependent on the value of the coherence function at each frequency ω. The function used in CIFER® software is:

$$W_\gamma(\omega) = \left[1.58\left(1 - e^{-\gamma_{xy}^2}\right)\right]^2 \tag{8.4}$$

thereby emphasizing the most reliable data. For a coherence of $\gamma_{xy}^2 = 0.6$, this function reduces the weight on the squared errors by 50%.

2. W_g and W_p are the relative weights for magnitude and phase squared errors. The normal convention is to use the values

$$W_q = 1.0 \tag{8.5a}$$

$$W_p = 0.01745 \tag{8.5b}$$

which sets 1 dB magnitude error comparable with 7.57° phase error.

As a guideline, a cost function of

$$J \leq 100 \tag{8.6}$$

generally reflects an acceptable level of accuracy for flight-dynamics modeling. [1]

9 State-space model identification

In many applications, the required end product of system identification is a state-space model expressed in terms of aerodynamic stability and control derivatives or even the physical system parameters as written in equations (3.3). State-space identification results are also very useful for simulation model validation or control system design, as shown in this thesis.

Initial guesses for the model parameters can be obtained from previous transfer-function identification results or from a-priori estimates based on first principles. [1]

The matrices $\mathbf{M}, \mathbf{F}, \mathbf{G}$ contain model parameters to be identified, but can also contain a-priori model parameters and constants (e.g. gravity g).

Once the identification parameters are determined, the model equations are easily expressed in conventional state-space form:

$$\dot{\mathbf{x}} = \mathbf{A}\mathbf{x} + \mathbf{B}\mathbf{u} \tag{9.1a}$$

$$\mathbf{y} = \mathbf{C}\mathbf{x} + \mathbf{D}\mathbf{u} \tag{9.1b}$$

where

$$\mathbf{A} = \mathbf{M}^{-1}\mathbf{F} \tag{9.2a}$$

$$\mathbf{B} = \mathbf{M}^{-1}\mathbf{G} \tag{9.2b}$$

$$\mathbf{C} = \mathbf{H_0} + \mathbf{H_1}\mathbf{M}^{-1}\mathbf{F} \tag{9.2c}$$

$$\mathbf{D} = \mathbf{H_1}\mathbf{M}^{-1}\mathbf{G} \tag{9.2d}$$

The form of (3.3) is chosen because if mass matrix terms $\mathbf{M}$ exist, this would result in elements of $\mathbf{A}$ and $\mathbf{B}$ matrices that are a complex combination of the desired physical parameters. [1]

9.1 MIMO state-space model identification

The identification is performed by comparing the resulting MIMO frequency responses of the state-space model with those of the flight data. The identification of MIMO state-space models is achieved by a direct extension of the SISO cost function (8.3) to matrix form. The identification cost function of the complete MIMO system (9.5) is simply the sum of the individual cost functions (8.3). [1]

The frequency response matrix of the identification model $\mathbf{H}(s)$ relates the Laplace transform of the output vector $\mathbf{y}$ to the Laplace transform of the input vector $\mathbf{u}$:

$$\mathbf{Y}(s) = \mathbf{H}(s)\mathbf{U}(s) \tag{9.3}$$

The frequency-response matrix of the model to be identified $\mathbf{H}(s)$ is expressed as a function of the state-space identification model matrices $\mathbf{M}, \mathbf{F}, \mathbf{G}, \mathbf{H_0}, \mathbf{H_1}$:

$$\mathbf{H}(s) = [\mathbf{H_0} + s\mathbf{H_1}]\left[(s\mathbf{I} - \mathbf{M^{-1}F})^{-1}\mathbf{M^{-1}G}\right] \tag{9.4}$$

The solution of the MIMO identification problem involves determining the model matrices $\mathbf{M}, \mathbf{F}, \mathbf{G}$ that produce a frequency response matrix $\mathbf{H}(s)$ that most closely matches the frequency responses obtained from the flight data $\hat{\mathbf{H}}_\mathbf{c}$. [1]

9.2 Cost function

Cost function, as suggested by Tischler[1], is analogous to the cost function of transfer-function extended to matrix form:

$$J = \sum_{l=1}^{n_{TF}} \left\{ \frac{20}{n_\omega} \sum_{\omega_1}^{\omega_{n_\omega}} W_\gamma \left[W_g(|\hat{T}_c| - |T|)^2 + W_p(\angle \hat{T}_c - \angle T)^2 \right] \right\}_l \tag{9.5}$$

where n_{TF} is number of selected frequency responses used for state-space identification.

As a guideline for acceptable state-space model identification, the average overall cost function

$$J_{ave} = \frac{J}{n_{TF}} \leq 100 \tag{9.6}$$

9.3 Accuracy analysis

The identification process returns the state-space model that best matches the frequency response flight data. A measure of accuracy or relative degree of confidence of the identification parameters (matrix elements) is needed for a number of reasons [1]:

1. The initial model structure usually needs to be refined.
2. A measure of parameter accuracy is needed to design a control system to ensure robustness.
3. Evaluation of differences between flight-test identified parameters and simulation parameters requires level of confidence.

9.3.1 Cramer-Rao inequality

The Cramer-Rao inequality CR_i can be viewed as "the minimum standard deviation σ_i in the parameter estimate, that would be obtained from many repeated maneuvers (test flights)".[1]

Thus

$$\sigma_i \geq CR_i$$

The relative values of the Cramer-Rao bounds among the identification parameters are very important for refining the model structure. Large relative Cramer-Rao bounds for individual parameters indicate poor identifiability and suggest that these parameters should be eliminated (or fixed) in the model structure.[1]

Cramer-Rao bounds are best expressed as a percentage of the converged identification values

$$\overline{CR}_i = \left| \frac{CR_i}{\Theta_i} \right| \times 100 \tag{9.7}$$

The CIFER® program refers to Cramer-Rao value as

$$2 \cdot CR_i \equiv \sigma_i$$

and suggests a guideline

$$\overline{CR}_i \leq 20\% \tag{9.8}$$

9.3.2 Insensitivity

Another accuracy measure, that is also a result of high Cramer-Rao bounds, which exceed guideline (9.8), is insensitivity.

High sensitivity occurs, when changes in a single parameter have little or no effect on converged cost function J, indicating that the parameter is not important in the selected model structure, and can be eliminated.[1]

Insensitivity is also best presented as normalized percentage of the converged parameter value

$$\bar{I}_i = \left| \frac{I_i}{\Theta_i} \right| \times 100\% \tag{9.9}$$

Again, CIFER® suggests a guideline

$$\bar{I}_i < 10\% \tag{9.10}$$

9.3.3 Example of system order reduction

This section presents the process of reducing the order of identified state-space model based on insensitivity and Cramer-Rao values.

Consider a system, with transfer function

$$H(s) = \frac{s+1}{(s+2)(s+1)}$$

and full state-space model

$$\mathbf{M_f} = \mathbf{I_2},\ \mathbf{F_f} = \mathbf{A_f} = \begin{bmatrix} -3 & -2 \\ 1 & 0 \end{bmatrix},\ \mathbf{G_f} = \mathbf{B_f} = \begin{bmatrix} 1 \\ 0 \end{bmatrix},\ \mathbf{H_{0f}} = \mathbf{C_f} = \begin{bmatrix} 1 & 1 \end{bmatrix},\ \mathbf{H_{1f}} = \mathbf{I_2}$$

It is quite obvious that this system can be reduced to

$$\mathbf{A_r} = \begin{bmatrix} -2 \end{bmatrix},\ \mathbf{B_r} = \begin{bmatrix} 1 \end{bmatrix},\ \mathbf{C_r} = \begin{bmatrix} 1 \end{bmatrix}$$

After exciting the full model in MATLAB®/Simulink® with frequency-sweep signal and following all steps mentioned in identification part of this thesis, frequency response data was obtained to be now used to identify state-space model.

The first iteration run of state-space identification process produced this result:

$$\mathbf{A_i} = \begin{bmatrix} -2.97 & -1.99 \\ 0.97 & 0.1 \end{bmatrix},\ \mathbf{B_i} = \begin{bmatrix} 1.85 \\ 0.86 \end{bmatrix},\ \mathbf{C_i} = \begin{bmatrix} 1 & 1 \end{bmatrix}$$

It seems quite similar to the full system used for identification, but first look on accuracy analysis shows, that although the achieved cost function is very good ($J = 0.0263 \leq 100$), the high Cramer-Rao and insensitivity values which break guidelines (9.8) and (9.10) suggest, that this system can be reduced.

Matrix element	Cramer-Rao [%]	Insensitivity [%]
a_{11}	$4.73 \cdot 10^3$	85.17
a_{12}	$1.11 \cdot 10^3$	$4.23 \cdot 10^3$
a_{21}	$4.68 \cdot 10^3$	83.65
a_{22}	$1.09 \cdot 10^3$	$3.07 \cdot 10^3$
b_{11}	$5.17 \cdot 10^3$	0.98
b_{21}	$1.12 \cdot 10^3$	2.13

Following the rules in Tischler[1], the parameter with the highest value of insensitivity (a_{12}) is set to zero and fixed (eliminated) in state-space model, and the identification process is repeated in such several iterations until all sensitivity values fulfill the guideline (9.10).

Then, same iteration process is repeated for Cramer-Rao values, until they fulfill guideline (9.8). This process of model structure reduction finally produces this satisfactory result:

$$\mathbf{A_i} = \begin{bmatrix} -1.99 \end{bmatrix},\ \mathbf{B_i} = \begin{bmatrix} 0.997 \end{bmatrix},\ \mathbf{C_i} = \begin{bmatrix} 1 \end{bmatrix}$$

Matrix element	Cramer-Rao [%]	Insensitivity [%]
a_{11}	15.65	4.59
b_{11}	6.21	1.82

10 Identification results

10.1 Longitudinal model

10.1.1 Data collection

Equilibrium point: $v_e = 260 \text{ kt} = 133.75 \text{ m/s},\ h_e = 10\,000 \text{ ft},\ \alpha_e = 6.2°,\ \theta_e = 6.2°$
Parameters of frequency-sweep excitation signal:

- frequency range of interest

$$[\omega_{min},\ \omega_{max}] = [0.03,\ 10] \text{ rad/s}$$

- filter cutoff and sampling frequency

$$\omega_f = 5 \cdot \omega_{max} = 50 \text{ rad/s} \approx 8 \text{ Hz}, \qquad F_s = 5 \cdot \frac{\omega_f}{2\pi} = 40 \text{ Hz}$$

- longest and shortest period of sweep signal

$$T_{min} = \frac{2\pi}{\omega_{max}} = 0.69 \text{ s}, \qquad T_{max} = \frac{2\pi}{\omega_{min}} = 209.44 \text{ s}$$

- record length

$$T_{rec} = 5 \cdot T_{max} = 1047.2 \text{ s}$$

Test flight began with 3s period in trim state, and then sweep was executed, followed by 3s trim state again at the end.

Three excitation test flights were performed for each longitudinal control input - el, thr and recorded time-histories concatenated into single data set per input.

Sweep was generated by computer (MATLAB®/ Simulink®) and manual joystick inputs were performed when needed to keep flight near selected equilibrium point.

Sweep signals had to be corrupted with white noise with amplitude of 10% of excitation signal to achieve more rich frequency spectrum around ω_{min}. This produced far better results (coherence at lower frequencies) than clean, noise-free sweep signals.

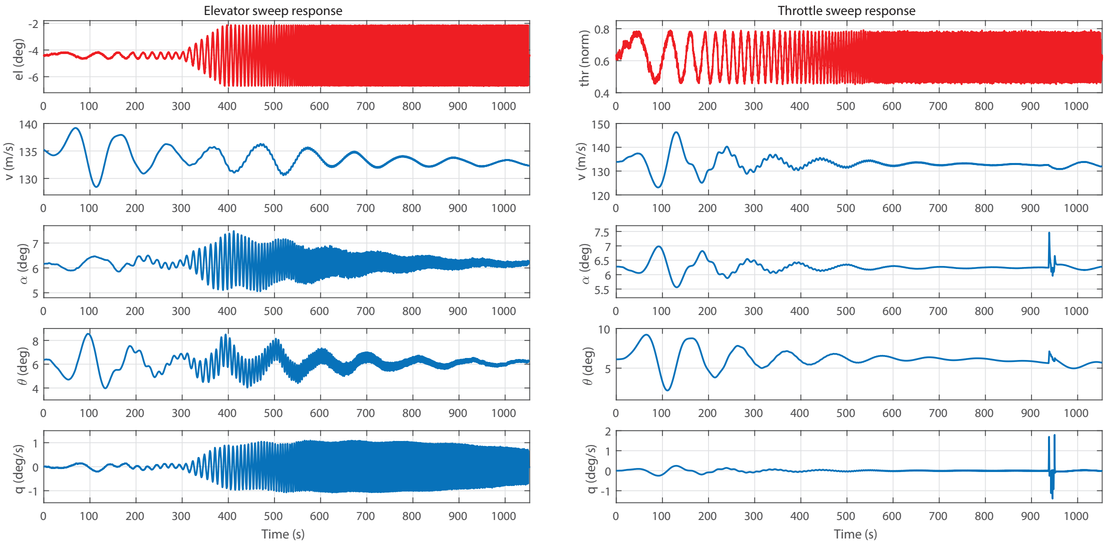

(a) Elevator sweep

(b) Throttle sweep

Figure 12: Collected longitudinal data

10.1.2 Data consistency

The first step in CIFER® program is to check data consistency of pitch-rate q and pitch-angle θ, which is product of q integration.

Identified frequency response $\frac{\theta_m}{q_m}$ is first visually compared with frequency response of ideal integrator $\frac{1}{s}$, which is shown in figure bellow.

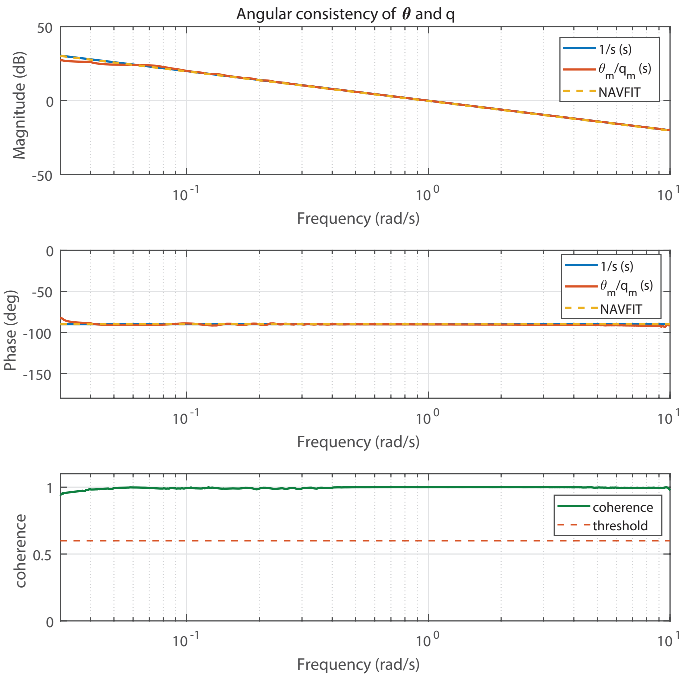

Figure 13: Angular consistency of θ and q

The yellow dashed line in magnitude and phase graph is another step of data consistency verification, namely identification of SISO transfer-function $H_i(s) = \frac{\theta_m}{q_m}(s)$, as described in section 6.

Transfer-function of ideal integrator:

$$H(s) = \frac{1}{s}$$

Identified transfer-function (curve fit):

$$H_i(s) = \frac{\theta_m}{q_m}(s) = \frac{K \cdot e^{-\tau s}}{s}(s) = \frac{0.978 \cdot e^{-0.0037s}}{s}, \qquad J = 14.492 \leq 100$$

The identified transfer-function is very close to transfer-function of ideal integrator $H(s)$, with acceptable value of cost function J fulfilling guideline (8.6) . Therefore, measurements of θ and q are kinematically consistent.

10.1.3 SISO frequency responses

Next step of system identification is SISO frequency responses, that is, to identify from acquired time-histories magnitude and phase plots for each input/output pair and it's corresponding coherence function - level of accuracy.

For frequency response identification, 5 windows A,B,C,D,E are used with lengths ranging from $T_{win_{min}} = 20 \cdot (2\pi)/\omega_{max} = 13$ s to $T_{win_{max}} = 0.5 \cdot T_{rec} = 523$ s, as explained in section 7.4. Results can be seen in figure 14 for elevator and figure 15 for throttle input. Long windows produce higher value coherence function and therefore better identification accuracy at lower frequencies, while on the other hand, shorter windows produce higher values coherence and better accuracy at higher frequencies.

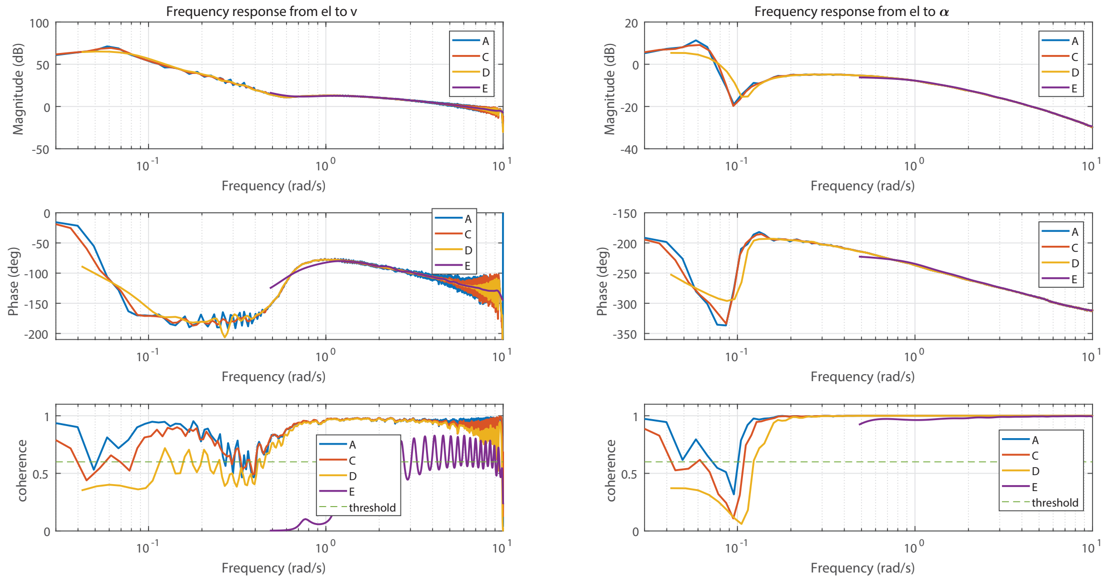

(a) v,alpha

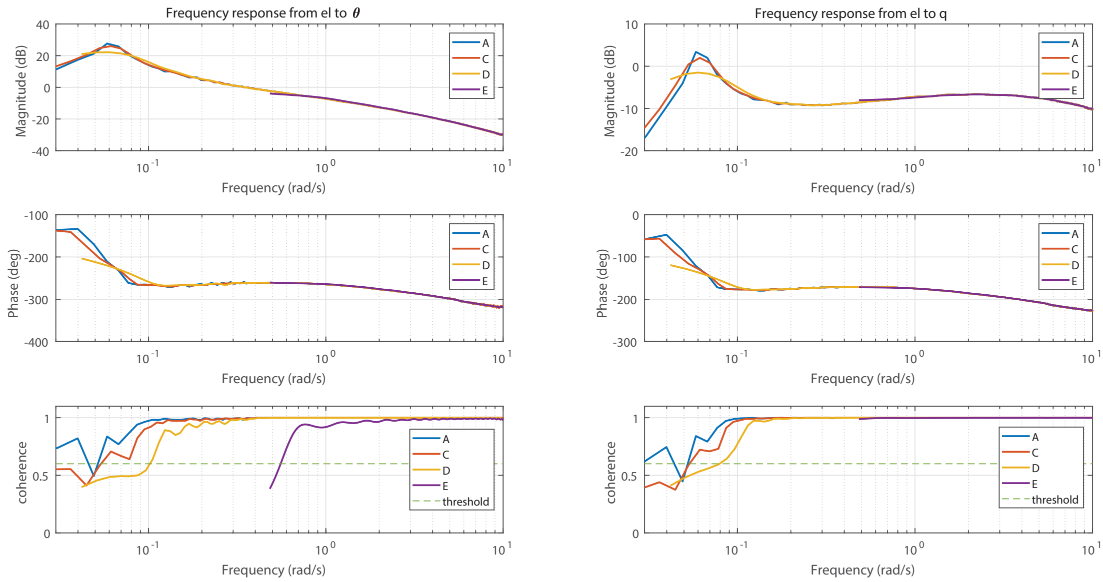

(b) theta,q

Figure 14: Frequency responses from elevator for 4 different window lengths

It can be seen in figure 15 that identification accuracy (coherence) is not very acceptable ($\gamma < 0.6$) in this case except airspeed output v. This can be explained by very low or almost none response of α, θ, and q to throttle excitation input.

The advantage of frequency response identification method is that this data (or only their selected frequency ranges) does not have to be used in further identification process, since it does not contribute any valuable information.

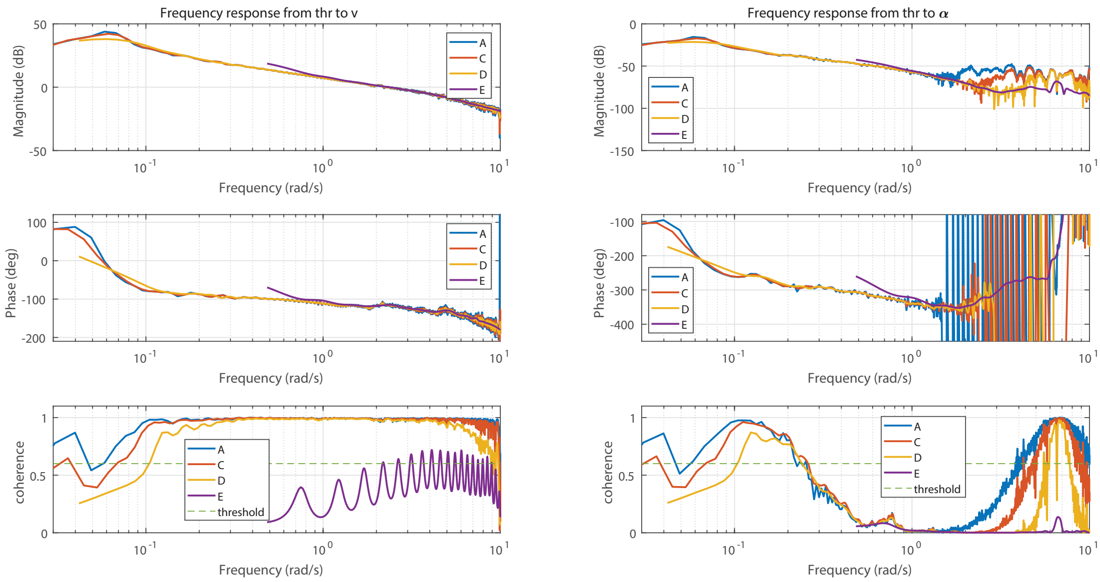

(a) v,alpha

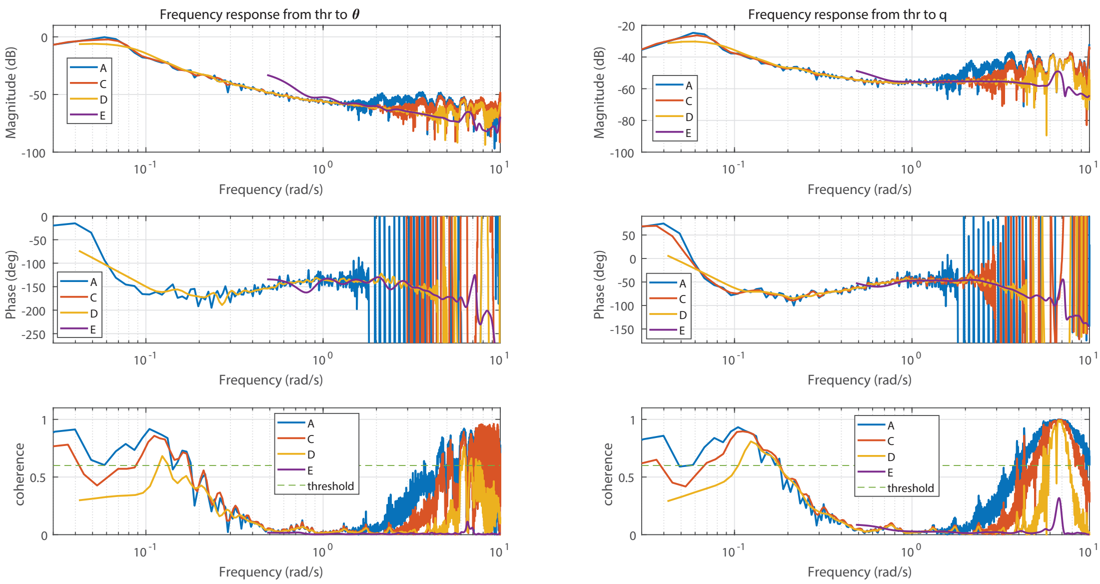

(b) theta,q

Figure 15: Frequency responses from throttle for 4 different window lengths

10.1.4 Composite windowing

Frequency response results for each window A,B,C,D,E obtained in previous identification step are now merged using composite windowing method described in section 7.4.2 and explained in more detail by Tischler [1].

Product of this method is SISO frequency response for each input/output pair of the model, with acceptable coherence at almost whole frequency range of interest.

Results from CIFER® are shown in figure 16 and 17 bellow, together with frequency responses obtained from MATLAB®/Identification Toolbox® for comparison.

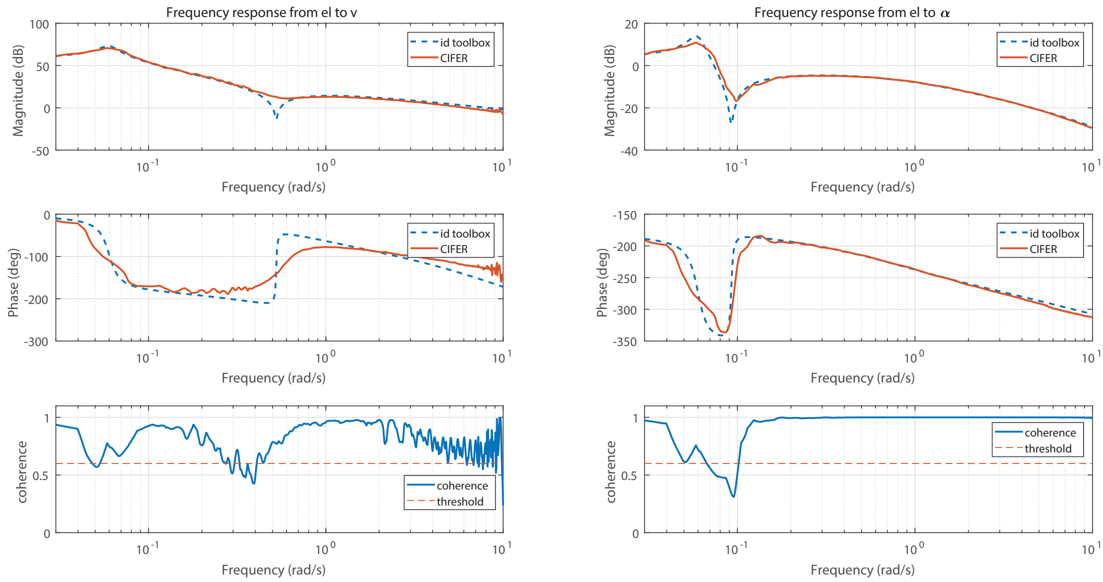

(a) v,alpha

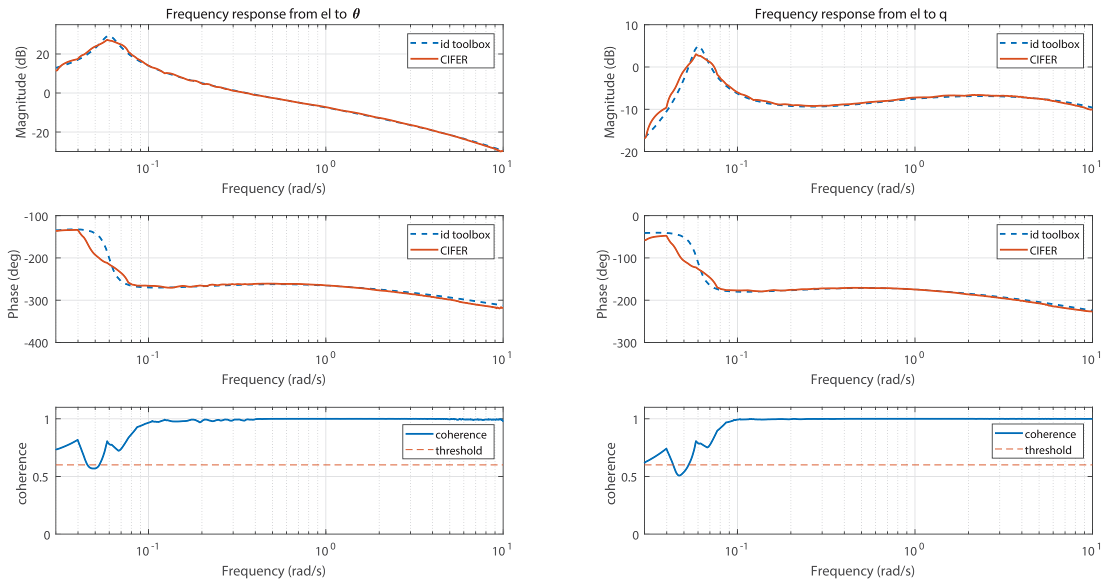

(b) theta,q

Figure 16: Composite frequency responses from elevator input

As mentioned in previous step, responses of α, θ and q from throttle does not have acceptable coherence at high frequencies or at all, so they will not be used in state-space identification process as it would corrupt final results rather than improve them.

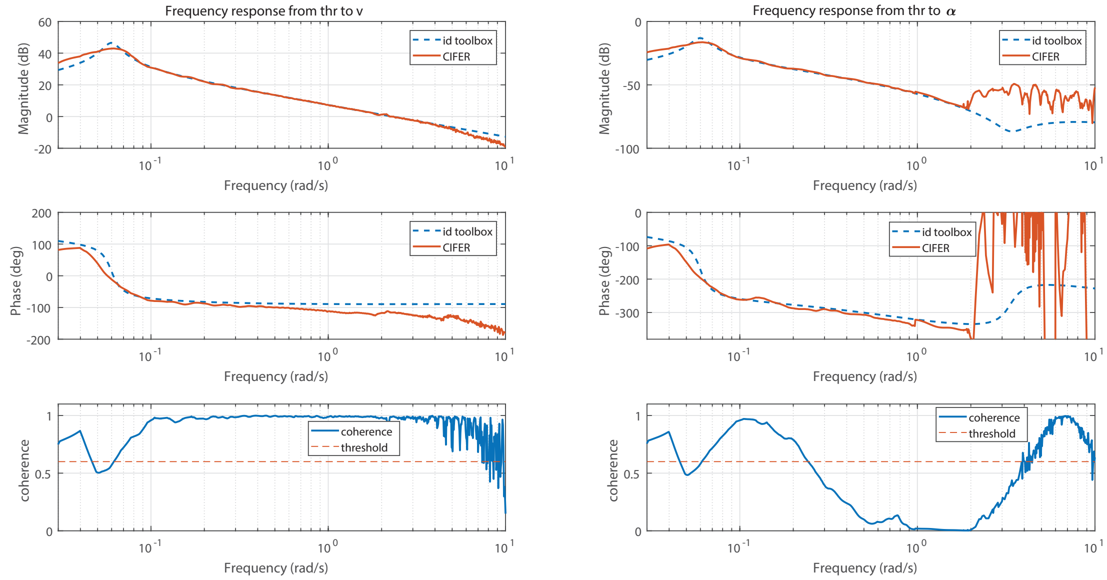

(a) v,alpha

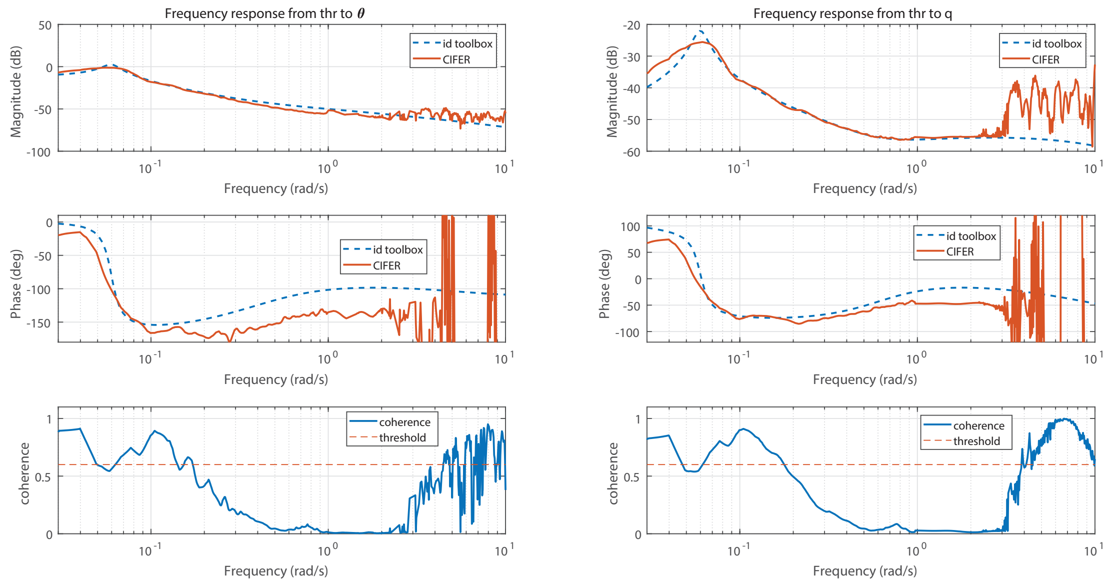

(b) theta,q

Figure 17: Composite frequency responses from throttle input

10.1.5 SISO transfer function

The last substep to the final identification result, which is MIMO state-space model, is identification of transfer-function of selected aircraft dynamics mode, in this case short-period approximation.

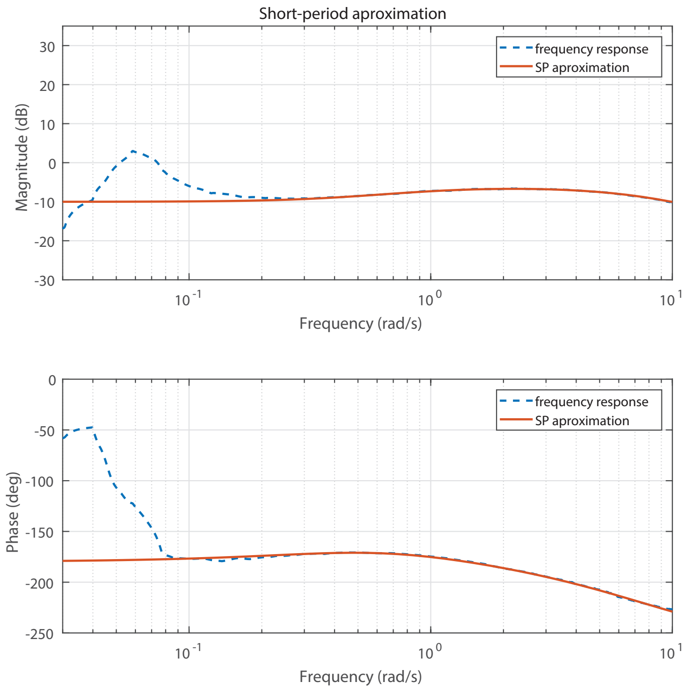

Figure 18: Transfer function identification of short-period mode

Short-period approximation is lower-order transfer function defined as [1]

$$\frac{q}{el}(s) = \frac{M_{el}(s+K)e^{-\tau s}}{[\zeta_{SP}, \omega_{SP}]} \tag{10.1}$$

where M_{el} is pitching moment due to elevator, ζ_{SP}, ω_{SP} are damping and frequency of this mode.

Using CIFER® for SISO transfer identification in selected frequency range of $[0.5,\ 10]$ rad/s, the short-period mode approximation is

$$\frac{q}{el}(s) = \frac{-4.07(s+0.514)}{(s+0.809)(s+8.194)}, \qquad J = 0.198 \leq 100$$

It is obvious from identification result, that two distinct negative poles mean that short-period mode of Concorde is overdamped.

Another important result is value of M_{el}.

$$M_{el} = -4.07$$

This value is just approximated, but it can be used as initial value for M_{el} in MIMO state-space model identification.

Approximated poles of short-period mode also give some insight of what to expect in further identification steps.

10.1.6 MIMO state-space model

The final step of frequency response identification method is MIMO state-space model identification.

Using SISO frequency responses obtained from composite windowing step and initial value of M_{el} from short-period approximation, state-space matrices are identified in the form of (3.3) by simultaneous fitting of estimated state-space model to selected frequency responses using cost function (9.5).

Frequency responses with not acceptable coherence, e.g. from throttle to α, θ and q, are dropped from this process, and of the remaining ones, only frequency ranges with acceptable coherence are used, e.g. response from elevator to θ or airspeed is mostly significant at lower frequencies, where phugoid mode is present, rather than in higher etc. This also improves final results.

Figures bellow show SISO frequency responses with simultaneous MIMO fit result:

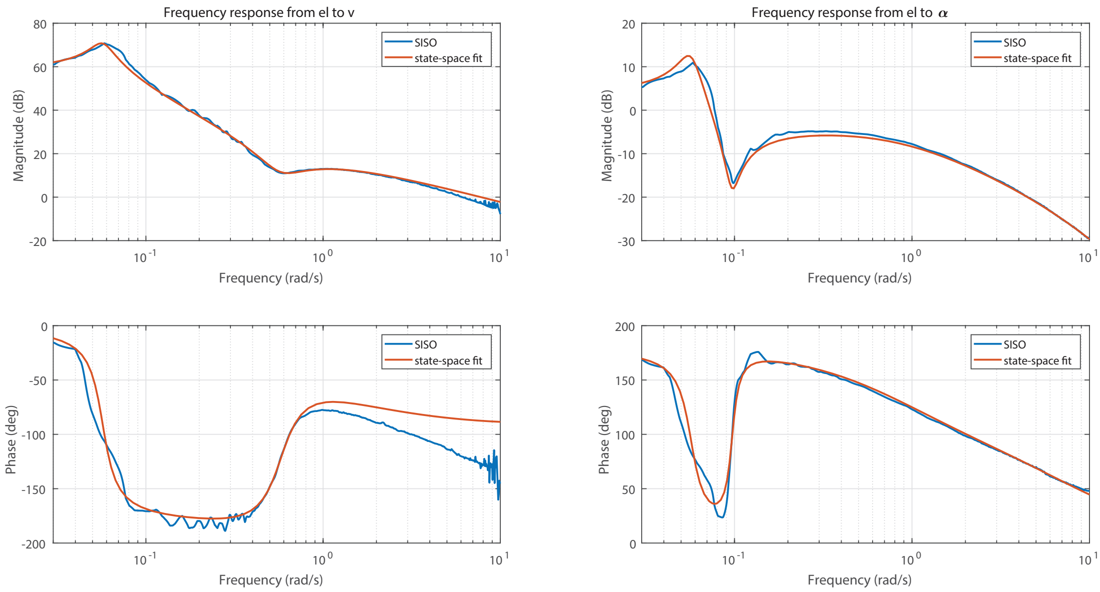

(a) v,alpha

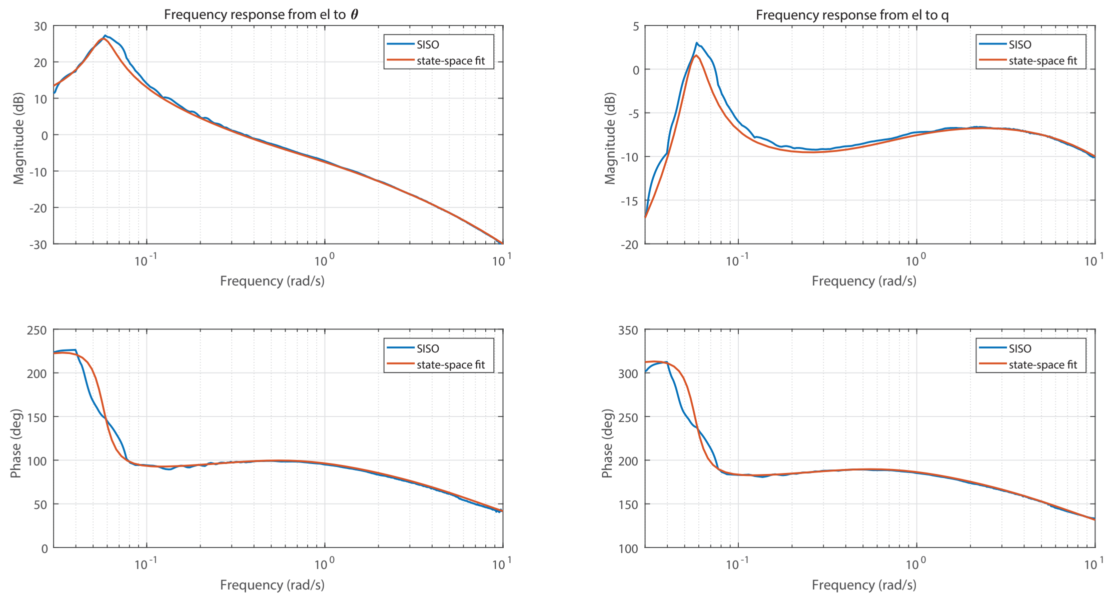

(b) theta,q

Figure 19: Longitudinal state-space frequency responses fit, elevator input

Fit of responses from throttle input to α, θ and q in figure 20 show that although they were not used in MIMO identification process, the frequency responses of resulted state-space model are quite close to former identified SISO responses, especially at lower frequencies.

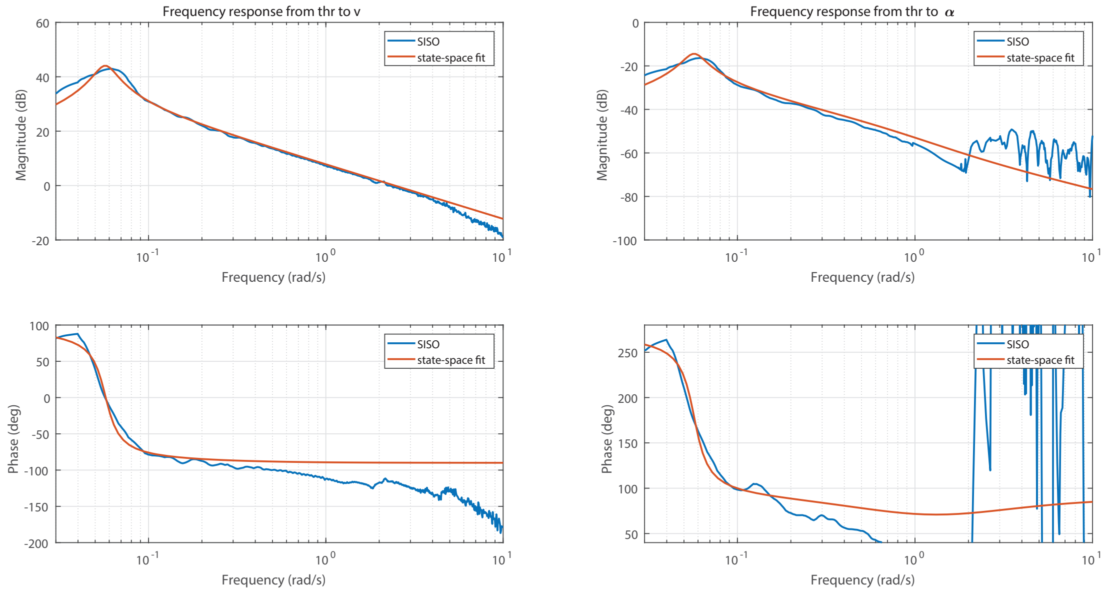

(a) v,alpha

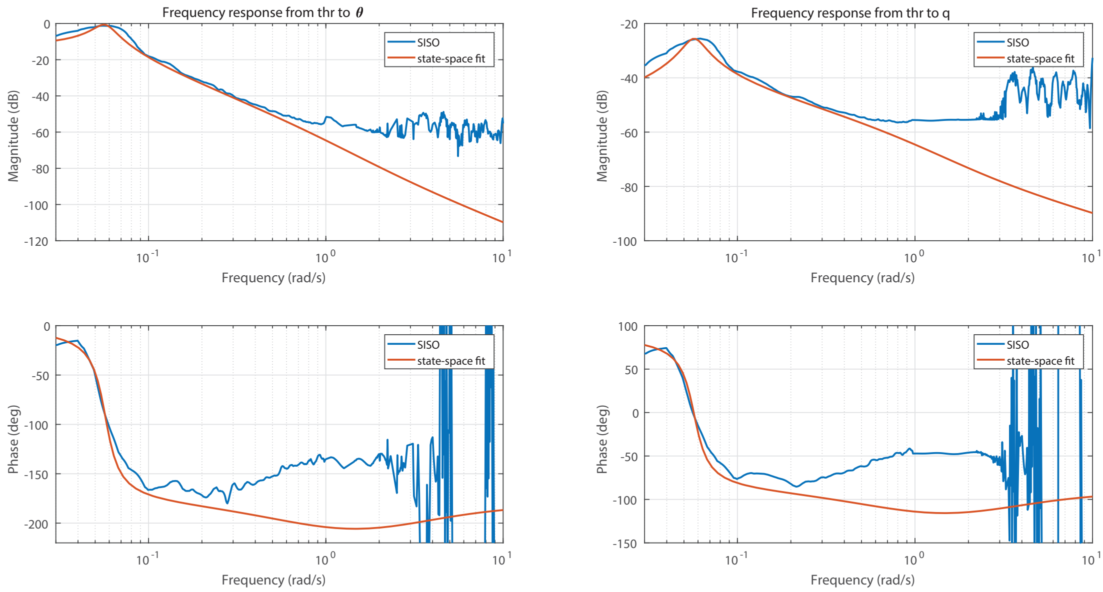

(b) theta,q

Figure 20: Longitudinal state-space frequency responses fit, throttle input

Another great advantage of frequency response identification methods and CIFER® program is, that desired form of state-space matrices of form (3.3) can be forced in identification process. For example, zeros, known constants such as g, v_e and trigonometric functions of very small values like flight-path angle γ, can be set and fixed (not to be changed during iteration fitting process) at appropriate places of matrices. Value of M_{el} identified in short-period approximation transfer- function is also used and fixed in matrix G at first, and then freed for finer estimation ($M_{el} = -4.07 \rightarrow -4.12$).

Bellow are identified state-space matrices of longitudinal aircraft model in selected equilibrium point:

$$\mathbf{M} = \begin{bmatrix} V_e - Z_{\dot\alpha} & 0 & 0 & 0 \\ -M_{\dot\alpha} & 1 & 0 & 0 \\ 0 & 0 & 1 & 0 \\ 0 & 0 & 0 & 1 \end{bmatrix} = \begin{bmatrix} 133 & 0 & 0 & 0 \\ 0 & 1 & 0 & 0 \\ 0 & 0 & 1 & 0 \\ 0 & 0 & 0 & 1 \end{bmatrix}$$

$$\mathbf{F} = \begin{bmatrix} Z_\alpha & V_e + Z_q & Z_V - X_{T_V}\sin(\alpha_e + \alpha_T) & -g_D \sin\gamma_e \\ M_\alpha + M_{T_\alpha} & M_q & M_V + M_{T_V} & 0 \\ X_\alpha & 0 & X_V + X_{T_V}\cos(\alpha_e + \alpha_T) & -g_D \cos\gamma_e \\ 0 & 1 & 0 & 0 \end{bmatrix} = \begin{bmatrix} -68.56 & 140.45 & -0.13 & 0 \\ -2.30 & -8.14 & 0 & 0 \\ 16.11 & 0 & 0.0015 & -9.81 \\ 0 & 1 & 0 & 0 \end{bmatrix}$$

$$\mathbf{G} = \begin{bmatrix} Z_{el} & -X_{thr}\sin(\alpha_e + \alpha_T) \\ M_{el} & M_{thr} \\ X_{el} & X_{thr}\cos(\alpha_e + \alpha_T) \\ 0 & 0 \end{bmatrix} = \begin{bmatrix} 0.13 & 0 \\ -4.12 & 0 \\ 7.35 & 2.43 \\ 0 & 0 \end{bmatrix}, \quad \mathbf{H_0} = \mathbf{I_4}, \quad \mathbf{H_1} = \mathbf{0}$$

The model is finally refined and it's accuracy analysis performed as suggested in section 9.3. Following table of accuracy analysis proves high quality of results.

Parameter	Identified Value	Cramer-Rao [%] (<20%)	Insensitivity [%] (<10%)
f_{11}	-68.56	6.95	1.41
f_{12}	140.45	4.82	1.14
f_{13}	-0.13	8.55	1.22
f_{21}	-2.30	8.66	1.67
f_{22}	-8.14	2.92	0.99
f_{31}	16.11	6.95	1.29
g_{31}	7.35	5.70	1.48
g_{32}	2.43	3.89	1.92

Table 4: Accuracy analysis of longitudinal state-space model

10.1.7 Comparison with MATLA®/Identification Toolbox®

Comparison of matrices, system poles and final frequency responses with results of MATLAB®/Identification Toolbox® is shown bellow. Although values of some parameters and shape of plots are quite similar, it is not true overall.

Moreover, there is no mechanism like Cramer-Rao bounds and insensitivity to analyze accuracy of individual matrix elements produced by Identification Toolbox®, which shows another advantage of frequency response methods utilized in CIFER®.

$$\mathbf{A_{CIF}} = \begin{bmatrix} -0.52 & 1.06 & -0.001 & 0 \\ -2.29 & -8.14 & 0 & 0 \\ 16.11 & 0 & 0.0015 & -9.81 \\ 0 & 1 & 0 & 0 \end{bmatrix}, \quad \mathbf{B_{CIF}} = \begin{bmatrix} 0.001 & 0 \\ -4.12 & 0 \\ 7.35 & 2.43 \\ 0 & 0 \end{bmatrix}$$

$$\mathbf{A_{idtbx}} = \begin{bmatrix} -0.53 & 0.99 & -0.0009 & -0.0027 \\ -2.38 & -9.84 & 0.0011 & 0.0069 \\ 14.84 & -35.06 & 0.0128 & -9.56 \\ 0.012 & 0.96 & 0 & 0 \end{bmatrix}, \quad \mathbf{B_{idtbx}} = \begin{bmatrix} -0.037 & -0.0016 \\ -4.60 & 0.017 \\ -7.22 & 2.35 \\ -0.019 & 0.0017 \end{bmatrix}$$

$$\mathbf{C} = \mathbf{I_4}, \quad \mathbf{D} = \mathbf{0}$$

Placement of poles confirms initial estimation of short-period mode, which is overdamped.

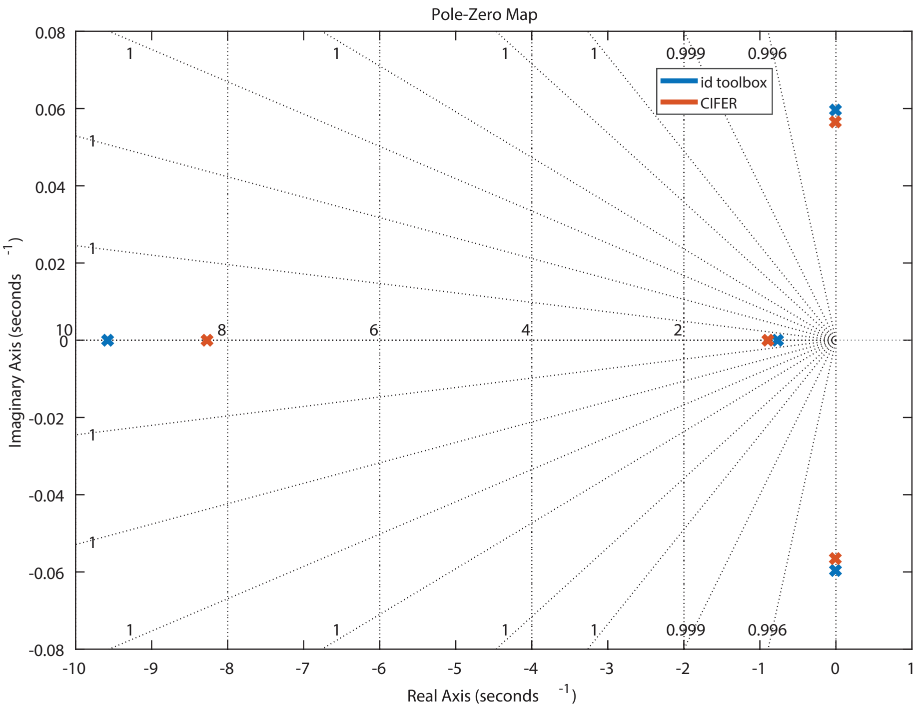

Figure 21: Comparison of longitudinal poles

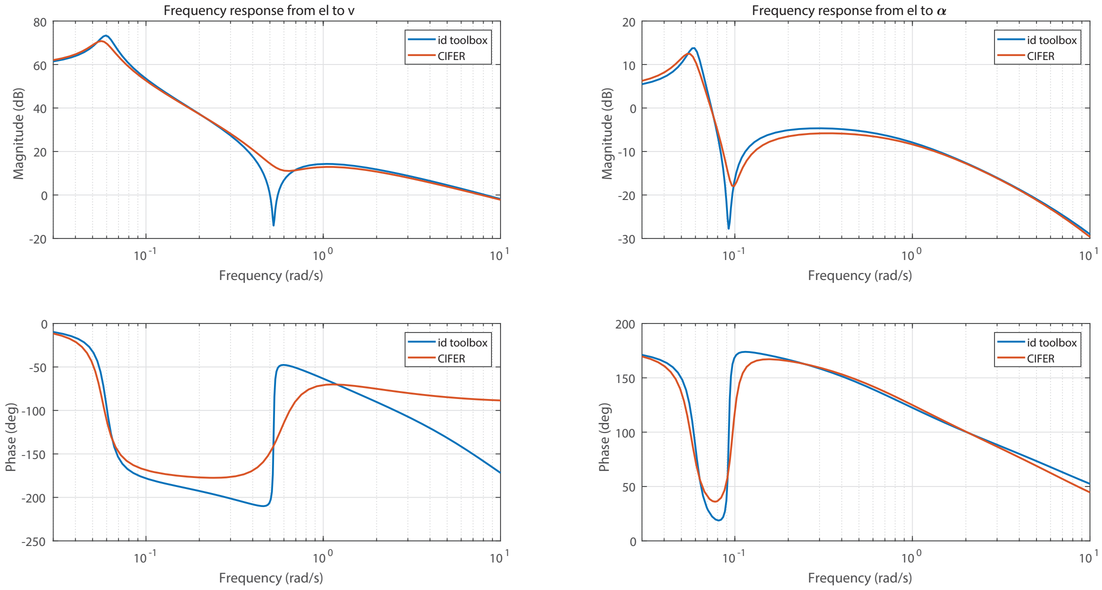

(a) v,alpha

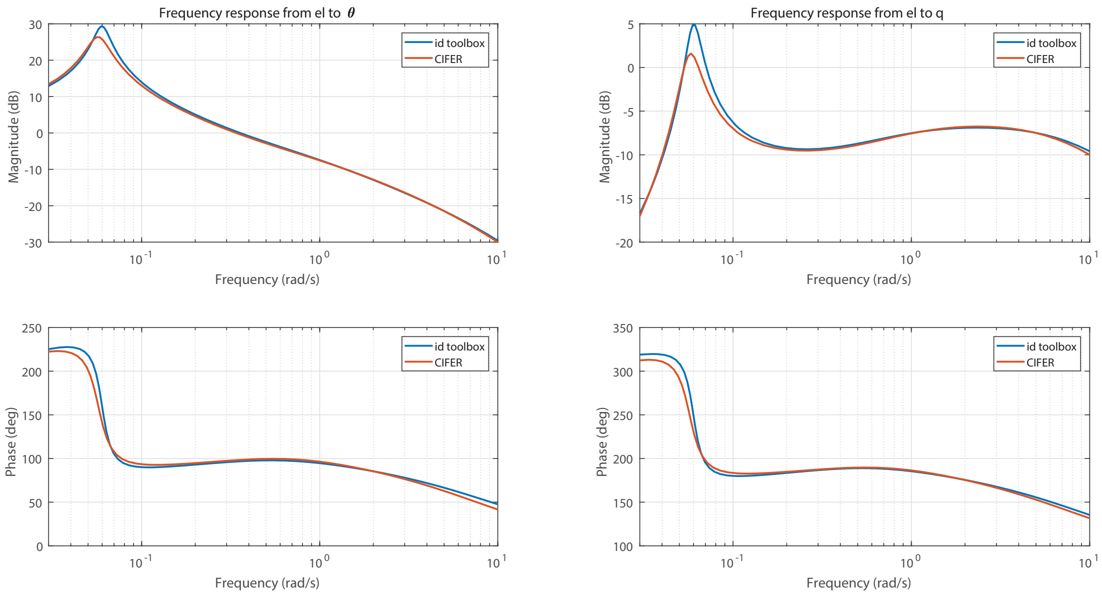

(b) theta,q

Figure 22: Comparison of MATLAB®/Identification Toolbox® with CIFER®, elevator input

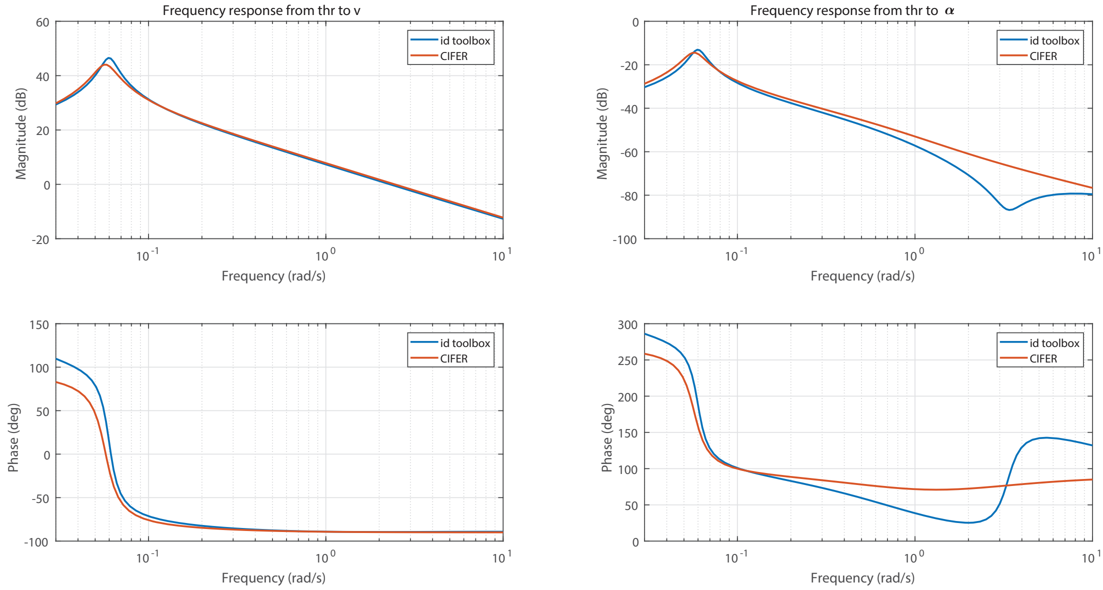

(a) v,alpha

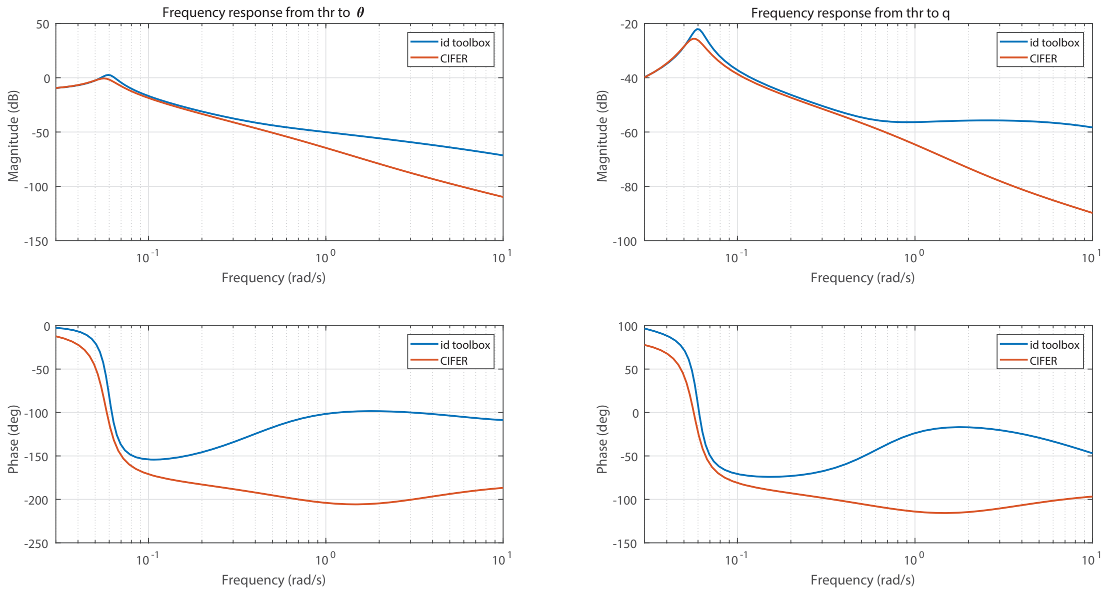

(b) theta,q

Figure 23: Comparison of MATLAB®/Identification Toolbox® with CIFER® , throttle input

Finally, figure bellow shows comparison of two identified state-space models using two different methods:
frequency response in CIFER and subspace in MATLAB®/Identification Toolbox®.

In verification process of identified models, it is very important to use different input signals that were used in excitation.

The figure compares responses to doublet input signals of both models with real-flight of Concorde in FlightGear simulator. Both models give acceptable results in terms of time-responses, except CIFER® results is far better in airspeed response.

However, being able to identify individual elements of state-matrices with desired structure and accuracy analysis can be required, for example, to properly identify aerodynamic parameters and derivatives of selected aircraft, which seems to be not possible with subspace methods.

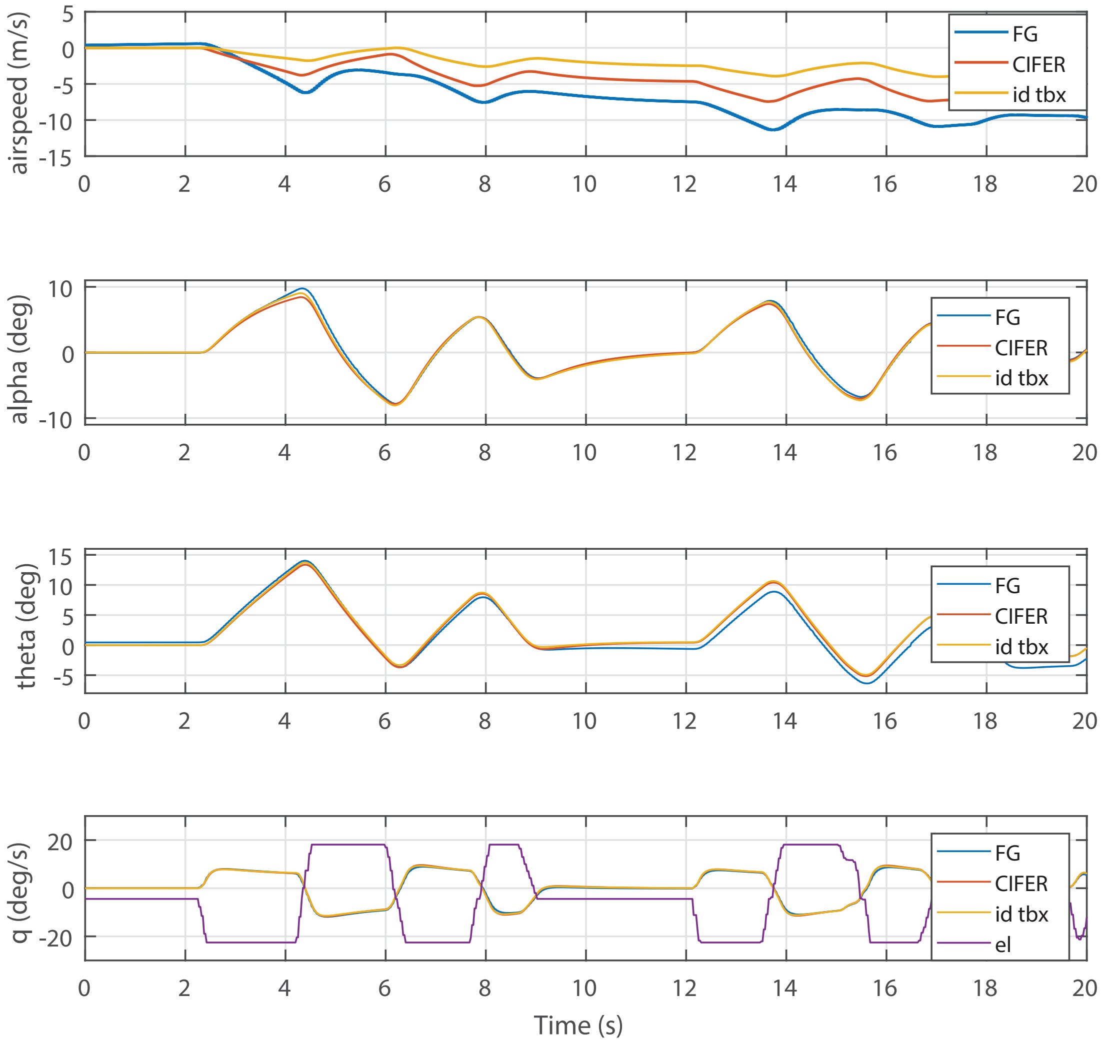

Figure 24: Comparison of identified model with simulator output

10.2 Lateral model

The very same procedure as in longitudinal model is used to identify lateral model with aileron and rudder inputs.

10.2.1 Data collection

Equilibrium point: $v_e = 260\ \text{kt} = 133.75\ \text{m/s},\ h_e = 10\,000\ \text{ft},\ \phi_e = 0°,\ \beta_e = 0°$

Parameters of frequency-sweep excitation signal:

- frequency range of interest

$$[\omega_{min},\ \omega_{max}] = [0.03,\ 10]\ \text{rad/s}$$

- filter cutoff and sampling frequency

$$\omega_f = 5 \cdot \omega_{max} = 50\ \text{rad/s} \approx 8\ \text{Hz}, \qquad F_s = 5 \cdot \frac{\omega_f}{2\pi} = 40\ \text{Hz}$$

- longest and shortest period of sweep signal

$$T_{min} = \frac{2\pi}{\omega_{max}} = 0.69\ \text{s}, \qquad T_{max} = \frac{2\pi}{\omega_{min}} = 209.44\ \text{s}$$

- record length

$$T_{rec} = 5 \cdot T_{max} = 1047.2\ \text{s}$$

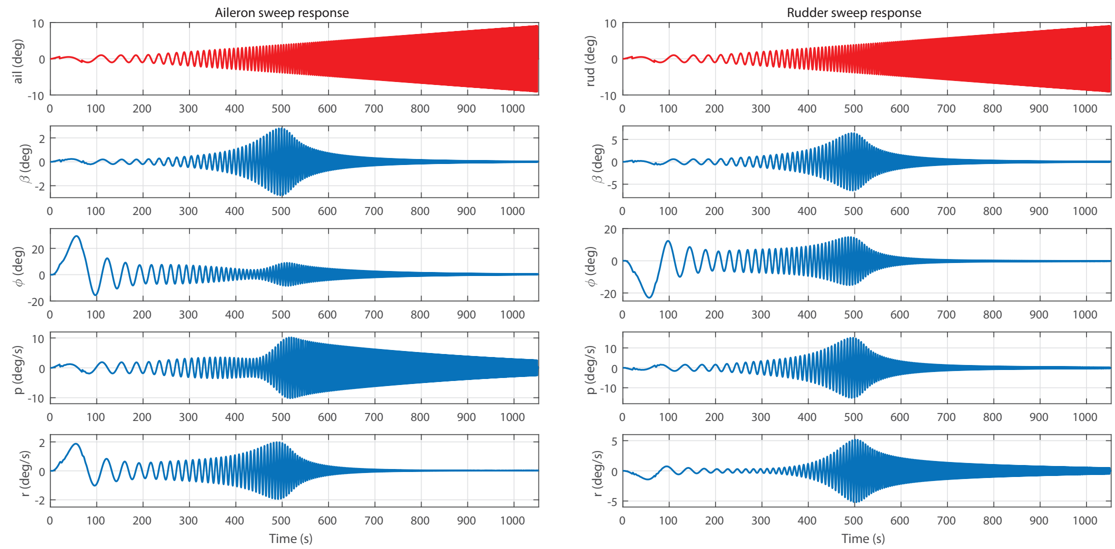

(a) Aileron sweep

(b) Rudder sweep

Figure 25: Collected lateral data

10.2.2 Data consistency

The first step in CIFER® program is to check data consistency of roll-rate p and roll-angle ϕ, which is product of p integration.

Identified frequency response $\frac{\phi_m}{p_m}$ is first visually compared with frequency response of ideal integrator $\frac{1}{s}$, which is shown in figure bellow.

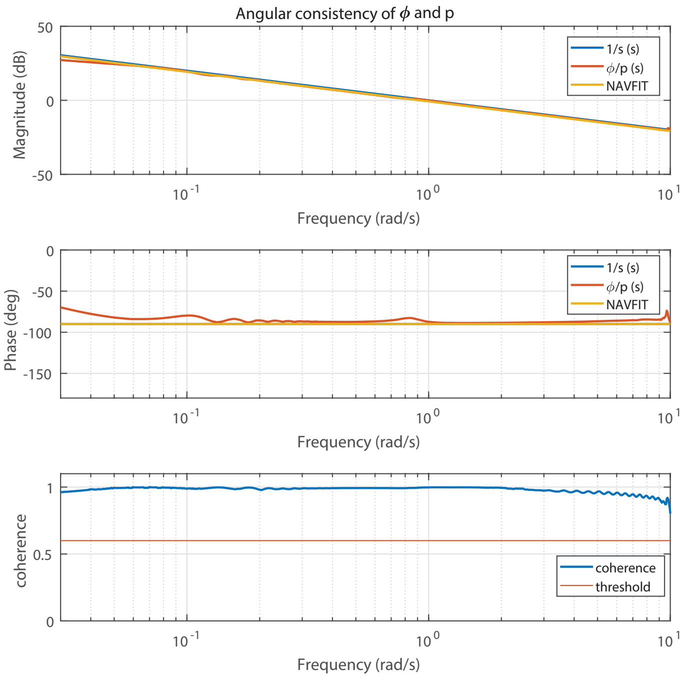

Figure 26: Angular consistency of ϕ and p

The yellow dashed line in magnitude and phase graph is another step of data consistency verification, namely identification of SISO transfer-function $H_i(s) = \frac{\phi_m}{p_m}(s)$, as described in section 6.

Transfer-function of ideal integrator:

$$H(s) = \frac{1}{s}$$

Identified transfer-function (curve fit):

$$H_i(s) = \frac{\phi_m}{p_m}(s) = \frac{K \cdot e^{-\tau s}}{s}(s) = \frac{0.9184}{s}, \qquad J = 23.346 \leq 100$$

The identified transfer-function is very close to transfer-function of ideal integrator $H(s)$, with acceptable value of cost function J fulfilling guideline (8.6) . Therefore, measurements of ϕ and p are kinematically consistent.

10.2.3 SISO frequency responses

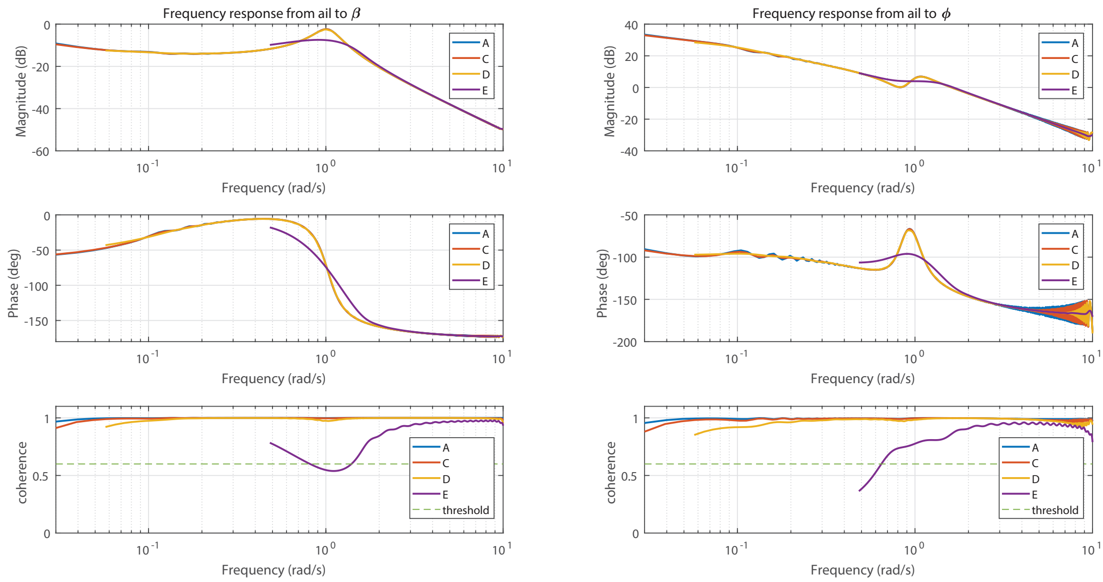

(a) beta,phi

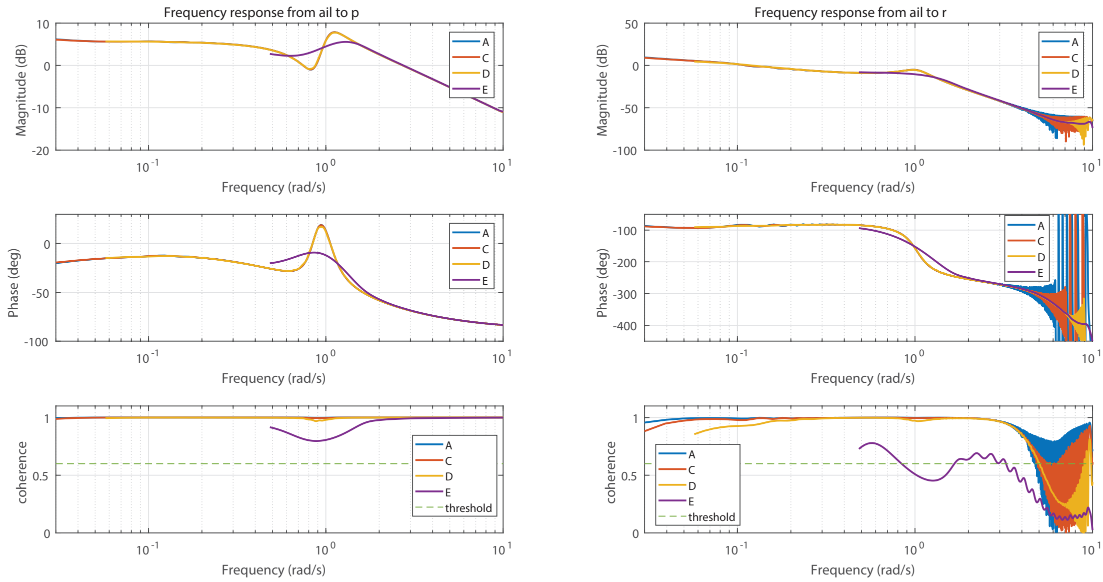

(b) p,r

Figure 27: Frequency responses from aileron for 4 different window lengths

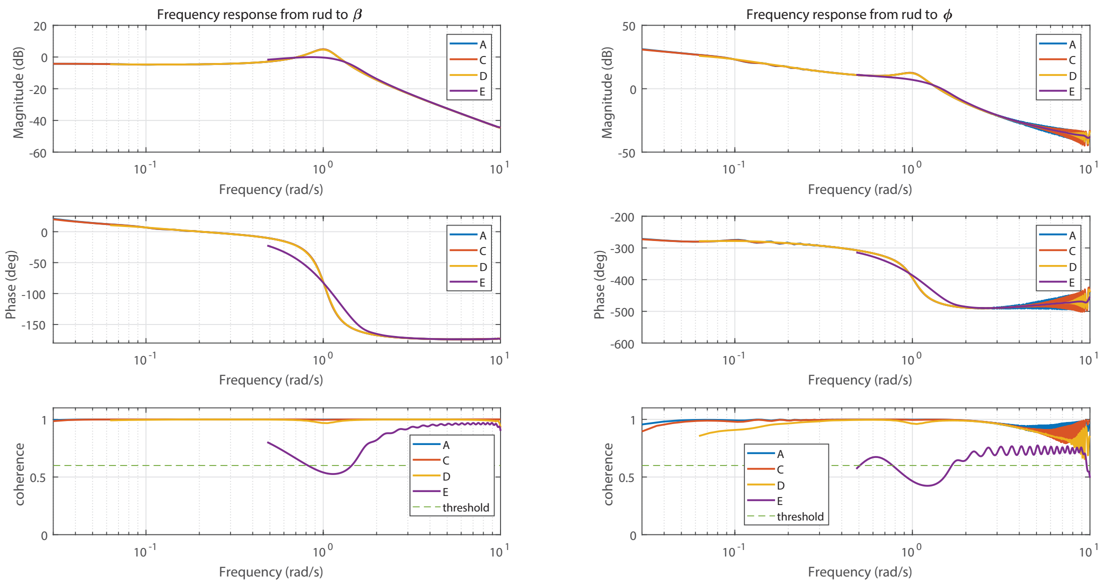

(a) beta,phi

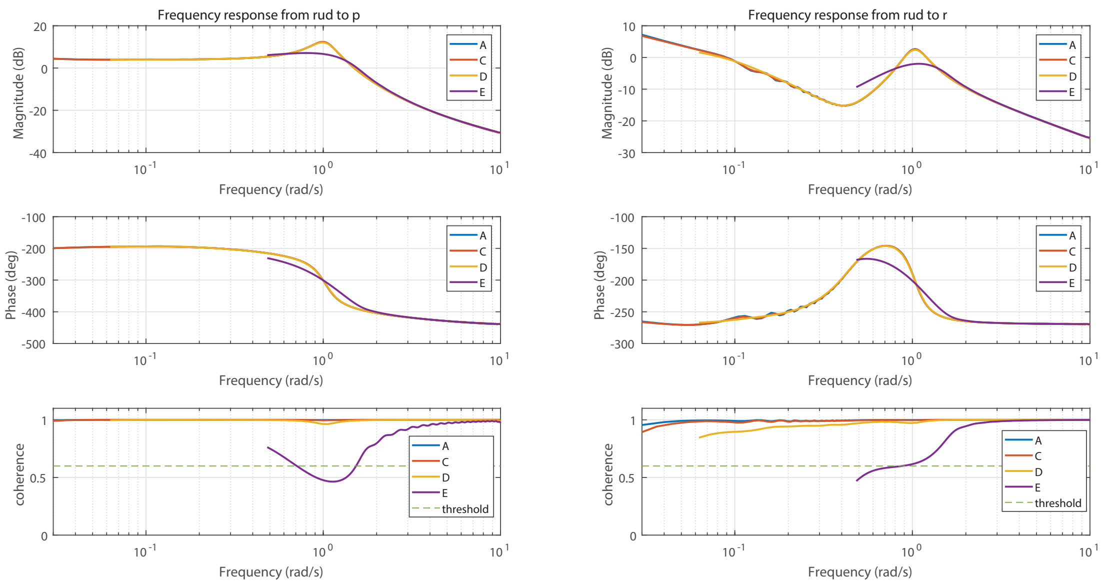

(b) p,r

Figure 28: Frequency responses from rudder for 4 different window lengths

10.2.4 Composite windowing

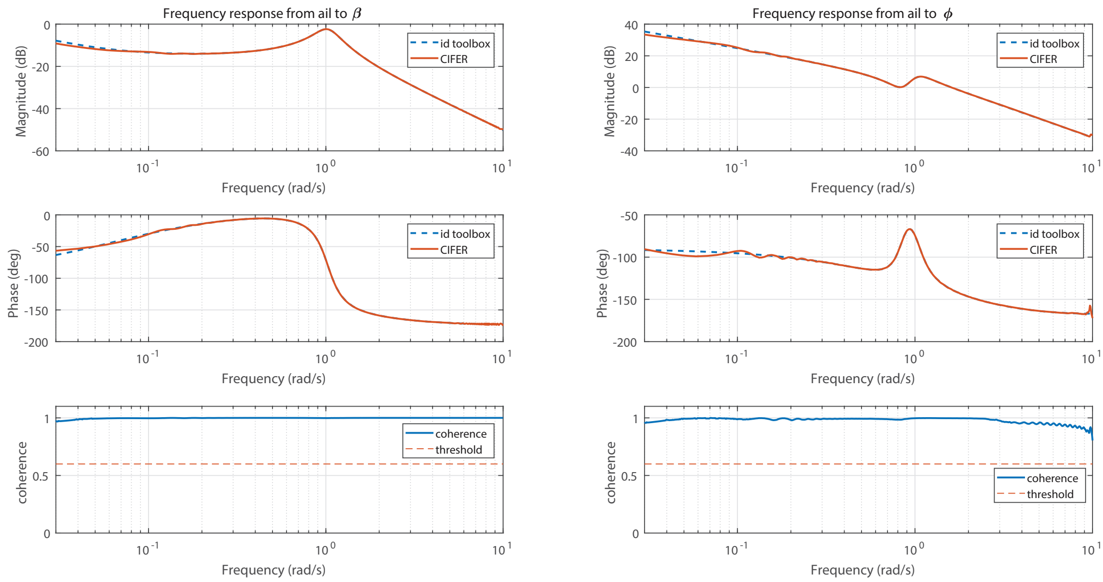

(a) beta,phi

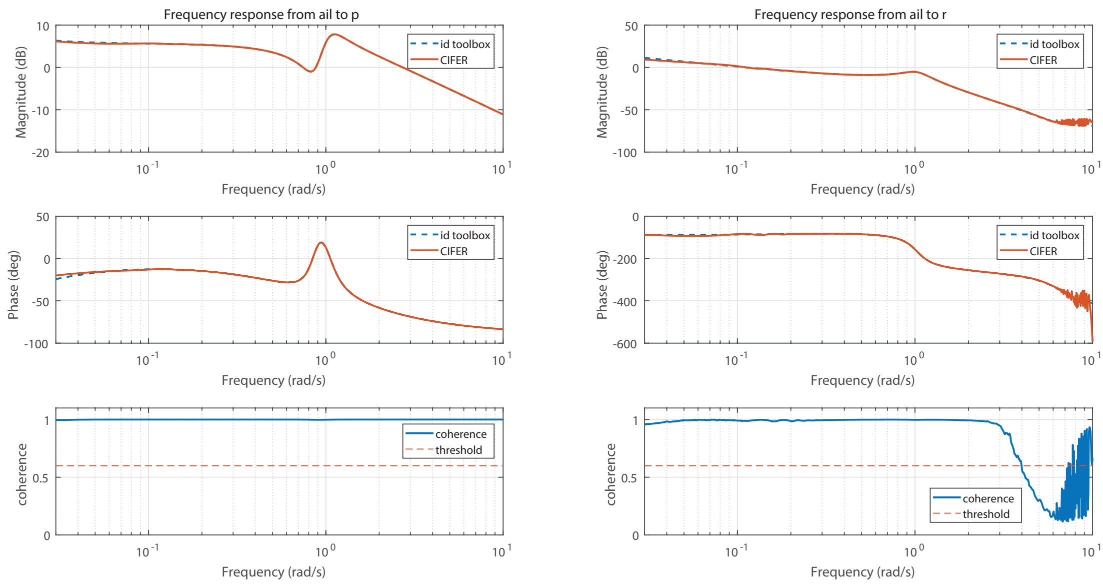

(b) p,r

Figure 29: Composite frequency responses from aileron input

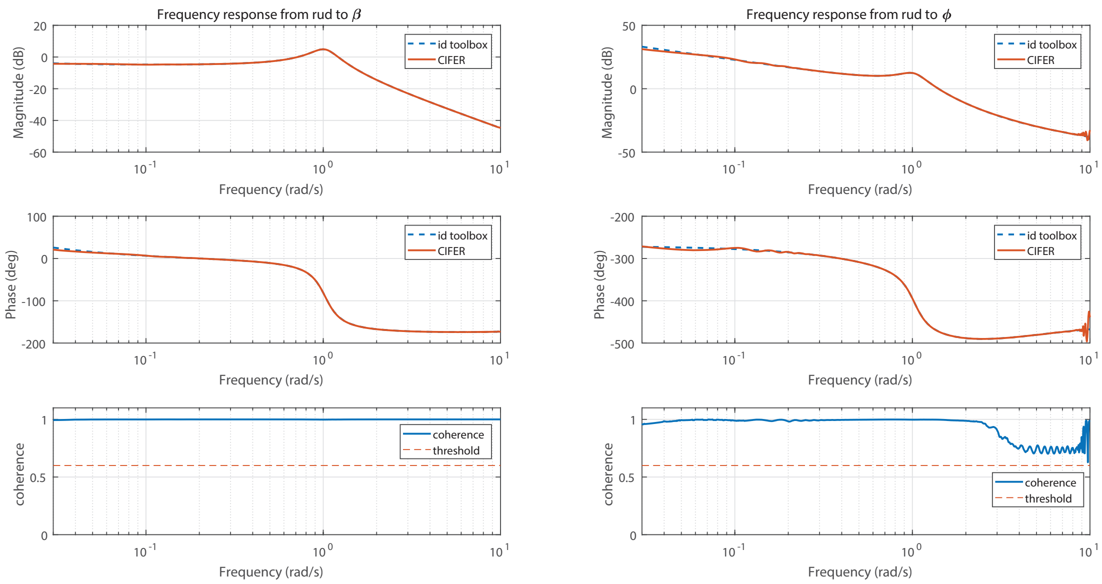

(a) beta,phi

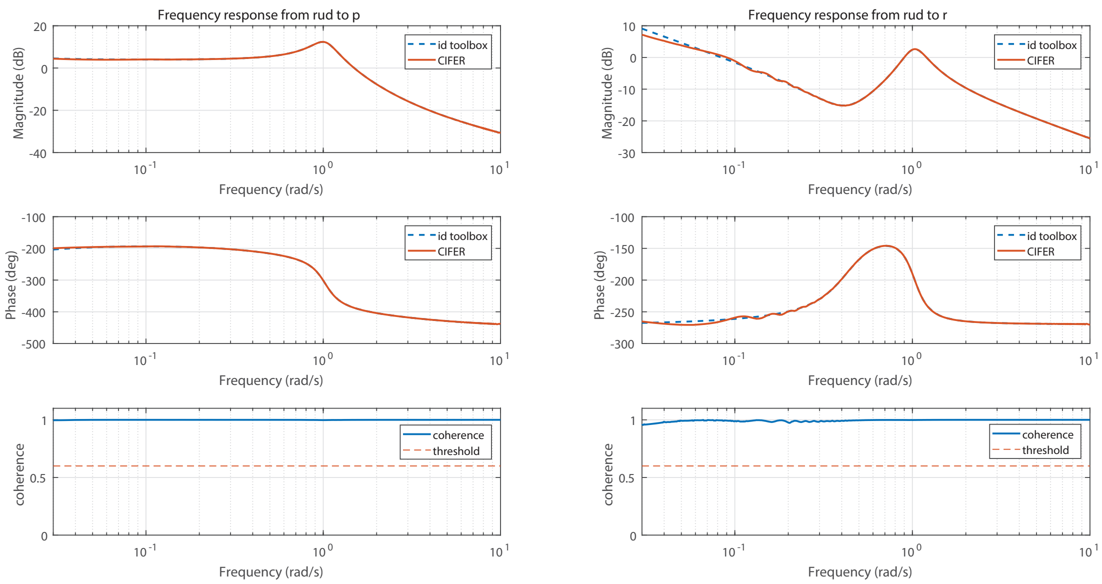

(b) p,r

Figure 30: Composite frequency responses from rudder input

10.2.5 SISO transfer function

The last substep to the final lateral identification result, which is MIMO state-space model, is identification of transfer-function of selected aircraft dynamics mode, in this case roll subsidence approximation.

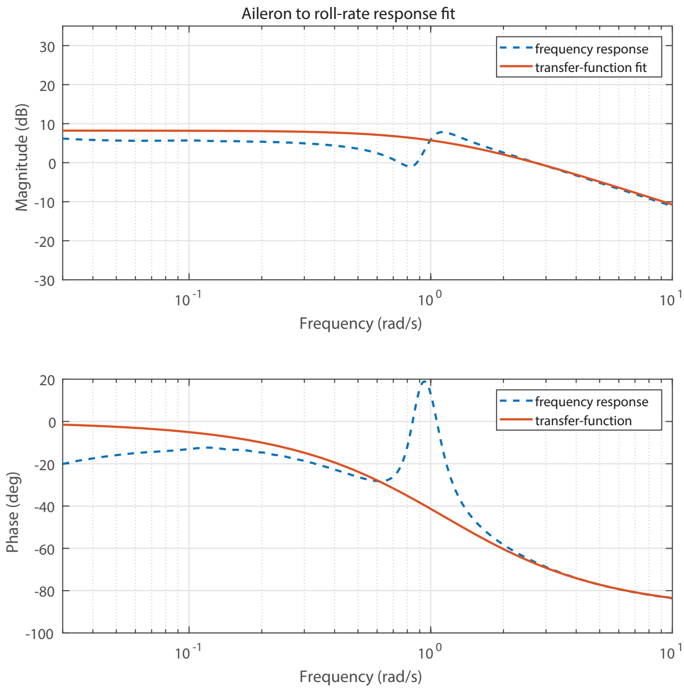

Figure 31: Transfer function identification of roll-response to aileron

Roll subsidence approximation is lower-order transfer-function defined as [1]

$$\frac{p}{ail}(s) = \frac{L_{ail}e^{-\tau s}}{(s + 1/T_r)} \tag{10.2}$$

where L_{ail} is rolling moment due to aileron, T_r is roll subsidence mode time constant and inverse of roll damping stability derivative $-L_p$.

Using CIFER® for SISO transfer-identification identification, the roll subsidence mode approximation is

$$\frac{p}{ail}(s) = \frac{2.928}{(s+1.137)}, \quad J = 5.264 \leq 100$$

$$1/T_r = -L_p \Rightarrow L_p = -1.137$$

$$L_{ail} = 2.928$$

Values of L_p and L_{ail} are just approximated, but they can be again used as initial values in MIMO state-space model identification.

Approximation of roll subsidence mode also gives some insight of what to expect in further identification steps.

10.2.6 MIMO state-space model

Figures bellow show SISO frequency responses with simultaneous MIMO fit result:

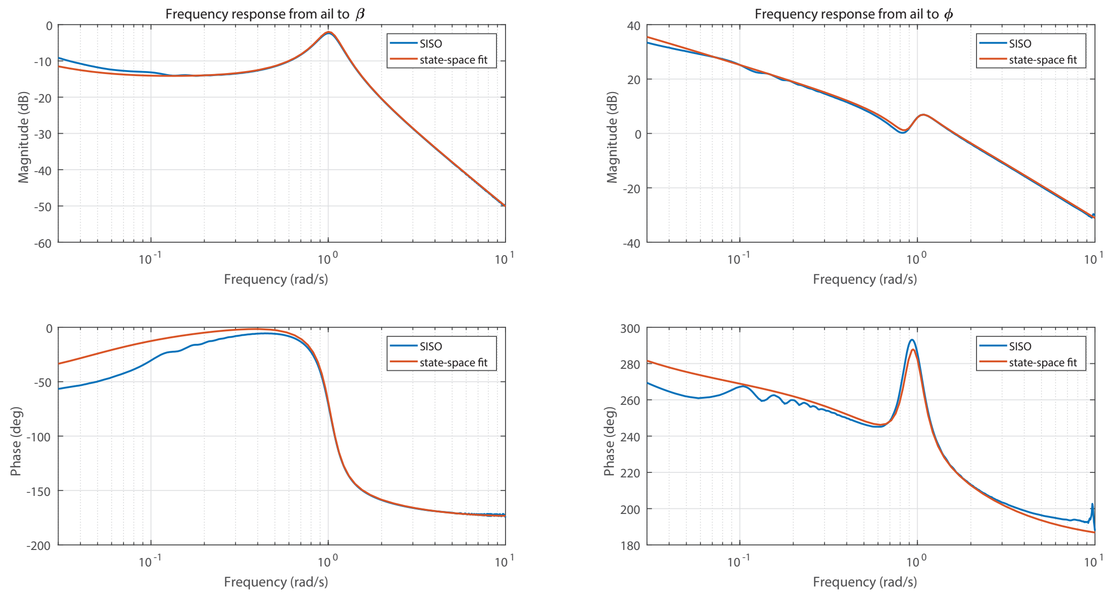

(a) beta,phi

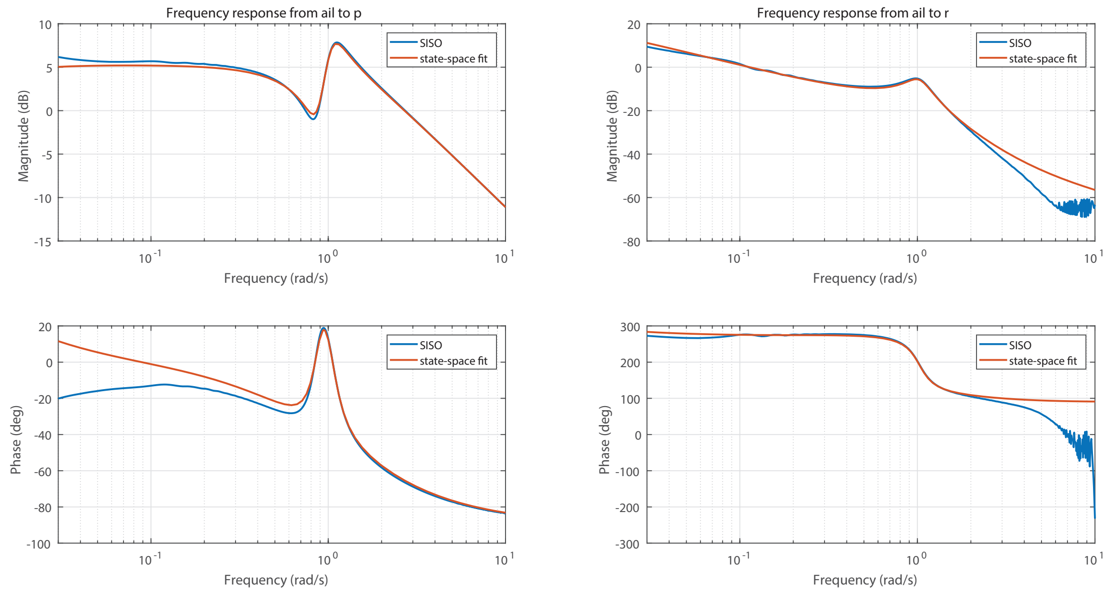

(b) p,r

Figure 32: Lateral state-space frequency responses fit, aileron input

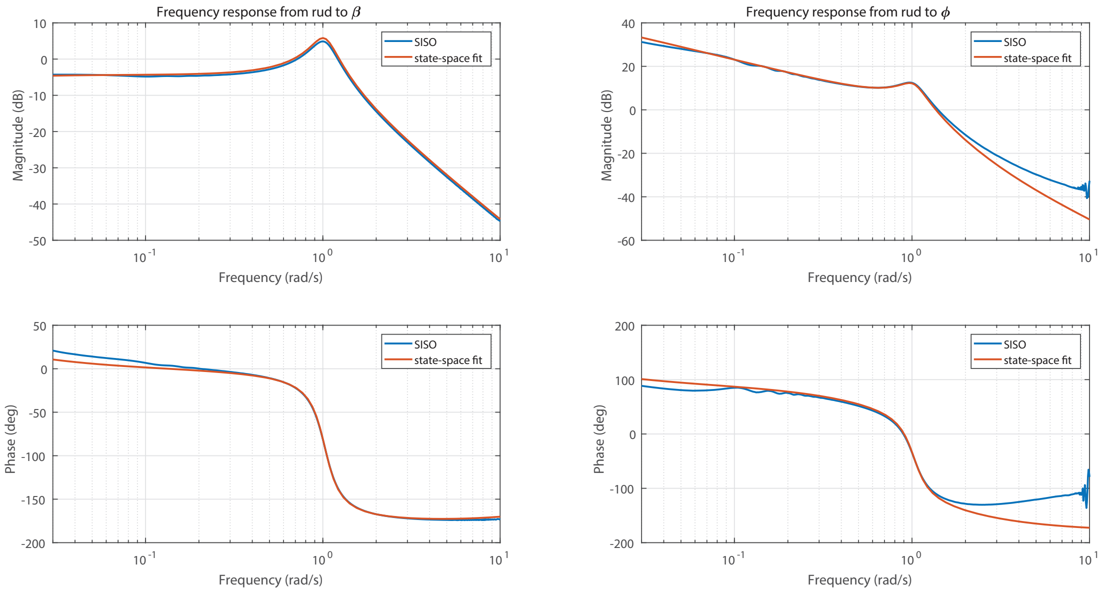

(a) beta,phi

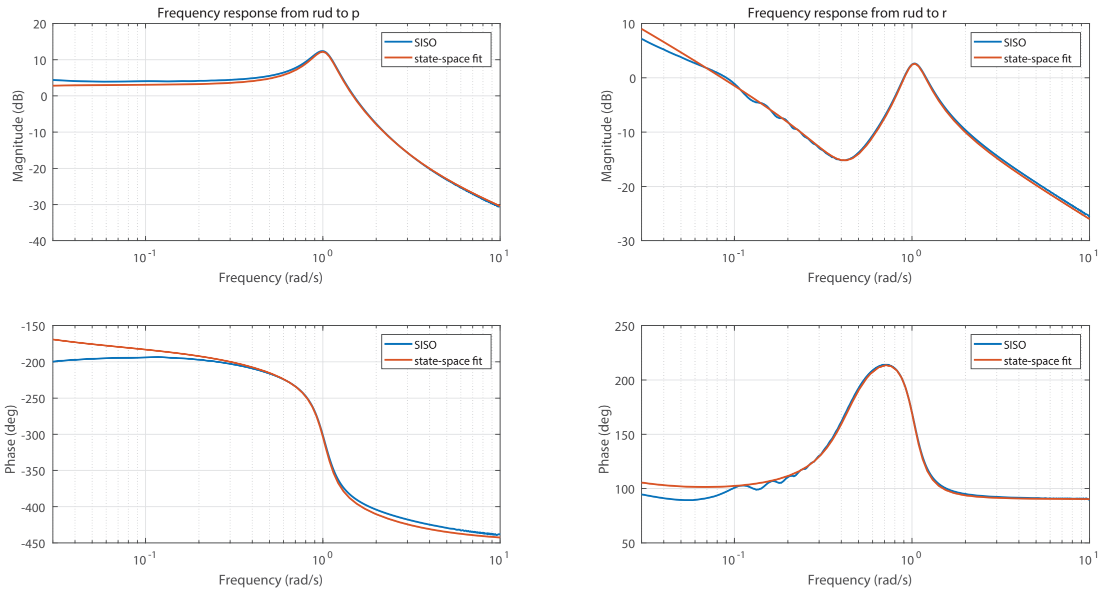

(b) p,r

Figure 33: Lateral state-space frequency responses fit, rudder input

Bellow are identified state-space matrices of lateral aircraft model in selected equilibrium point:

$$\mathbf{M} = \begin{bmatrix} V_e & 0 & 0 & 0 \\ 0 & 1 & 0 & 0 \\ 0 & 0 & 1 & 0 \\ 0 & 0 & 0 & 1 \end{bmatrix} = \begin{bmatrix} 133 & 0 & 0 & 0 \\ 0 & 1 & 0 & 0 \\ 0 & 0 & 1 & 0 \\ 0 & 0 & 0 & 1 \end{bmatrix}$$

$$\mathbf{F} = \begin{bmatrix} Y_\beta & g_D \cos\theta_e & Y_p & Y_r - V_e \\ 0 & 0 & c\gamma_e/c\theta_e & s\gamma_e/c\theta_e \\ L_\beta & 0 & L'_p & L_r \\ N_\beta & 0 & N'_p & N_r \end{bmatrix} = \begin{bmatrix} -26.39 & 9.81 & 14.53 & -155.61 \\ 0 & 0 & 1 & 0 \\ -3.26 & 0 & -1.19 & 0 \\ 0.66 & 0 & 0 & -0.031 \end{bmatrix}$$

$$\mathbf{G} = \begin{bmatrix} Y_{ail} & Y_{rud} \\ 0 & 0 \\ L_{ail} & L_{rud} \\ N_{ail} & N_{rud} \end{bmatrix} = \begin{bmatrix} 0 & 0 \\ 0 & 0 \\ 2.81 & 0.283 \\ 0 & -0.49 \end{bmatrix}, \quad \mathbf{H_0} = \mathbf{I_4}, \quad \mathbf{H_1} = \mathbf{0}$$

The model is finally refined and it's accuracy analysis performed as suggested in section 9.3. Following table of accuracy analysis again proves high quality of achieved result.

Parameter	Identified Value	Cramer-Rao [%] ($< 20\%$)	Insensitivity [%] ($< 10\%$)
f_{11}	-26.39	7.97	3.47
f_{13}	14.53	5.28	1.82
f_{14}	-155.61	3.27	0.80
f_{31}	-3.26	4.59	1.14
f_{33}	-1.19	12.38	2.70
f_{41}	0.66	3.45	0.75
f_{44}	-0.031	7.97	3.83
g_{31}	2.81	3.92	0.92
g_{32}	0.283	8.68	4.12
g_{42}	-0.49	3.30	0.91

Table 5: Accuracy analysis of lateral state-space model

10.2.7 Comparison with MATLAB/Identification Toolbox

Comparison of state-space matrices, system poles and final frequency responses with results of MATLAB®/Identification Toolbox® is shown bellow. Although values of some parameters and shape of plots are quite similar, it is not true overall.

$$\mathbf{A}_{\mathbf{CIF}} = \begin{bmatrix} -0.198 & 0.074 & 0.11 & -1.17 \\ 0 & 0 & 1 & 0 \\ -3.26 & 0 & -1.189 & 0 \\ 0.66 & 0 & 0 & -0.031 \end{bmatrix}, \ \mathbf{B}_{\mathbf{CIF}} = \begin{bmatrix} 0 & 0 \\ 0 & 0 \\ 2.81 & 0.283 \\ 0 & -0.49 \end{bmatrix}$$

$$\mathbf{A}_{\mathbf{idtbx}} = \begin{bmatrix} -0.145 & 0.063 & 0.11 & -1.01 \\ -0.11 & 0.001 & 0.93 & -0.2 \\ -3.52 & 0.013 & -1.13 & 0.38 \\ 0.72 & 0.001 & -0.009 & -0.09 \end{bmatrix}, \ \mathbf{B}_{\mathbf{idtbx}} = \begin{bmatrix} 0.002 & 0.005 \\ 0.03 & 0.11 \\ 2.79 & 0.27 \\ 0.005 & -0.53 \end{bmatrix}$$

$$\mathbf{C} = \mathbf{I_4}, \quad \mathbf{D} = \mathbf{0}$$

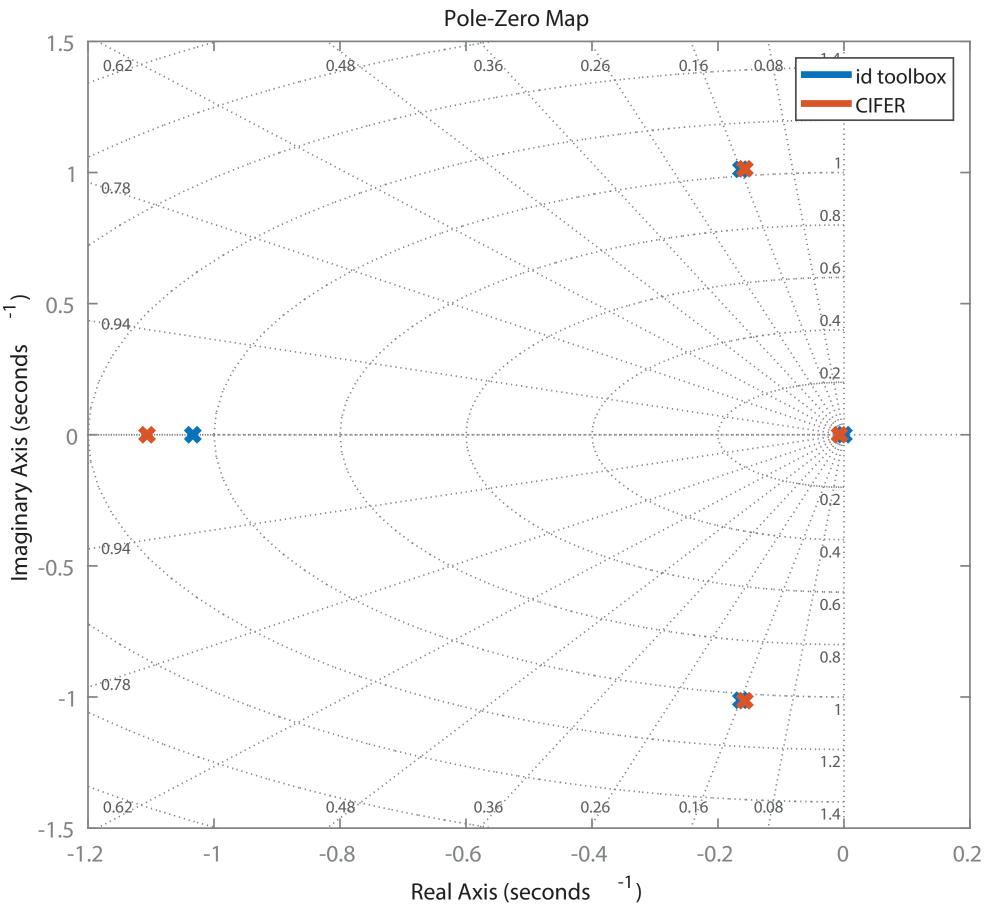

Figure 34: Comparison of lateral poles

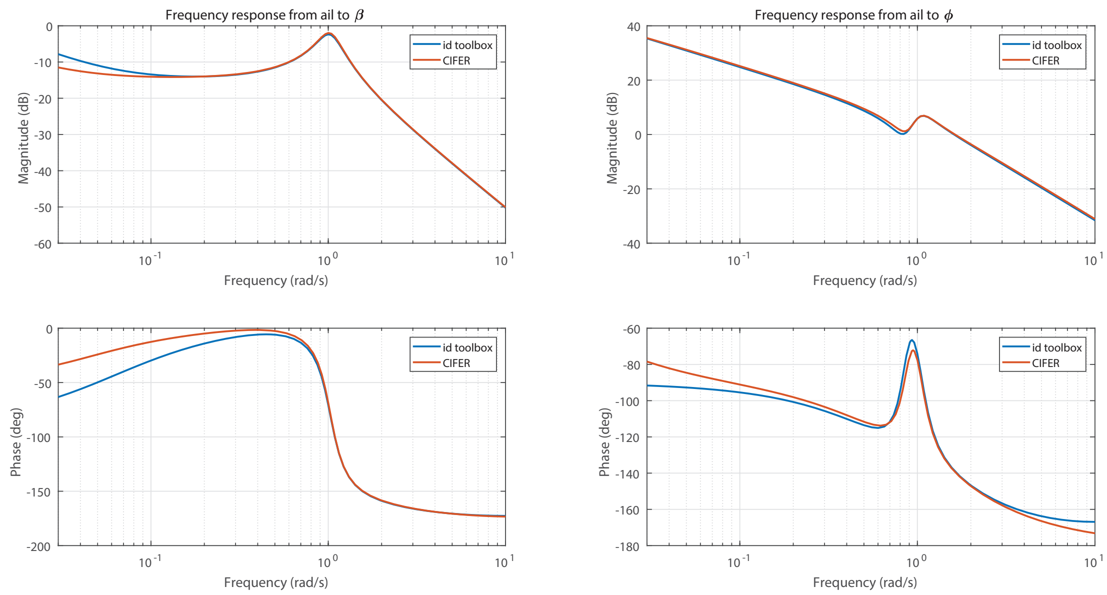

(a) beta,phi

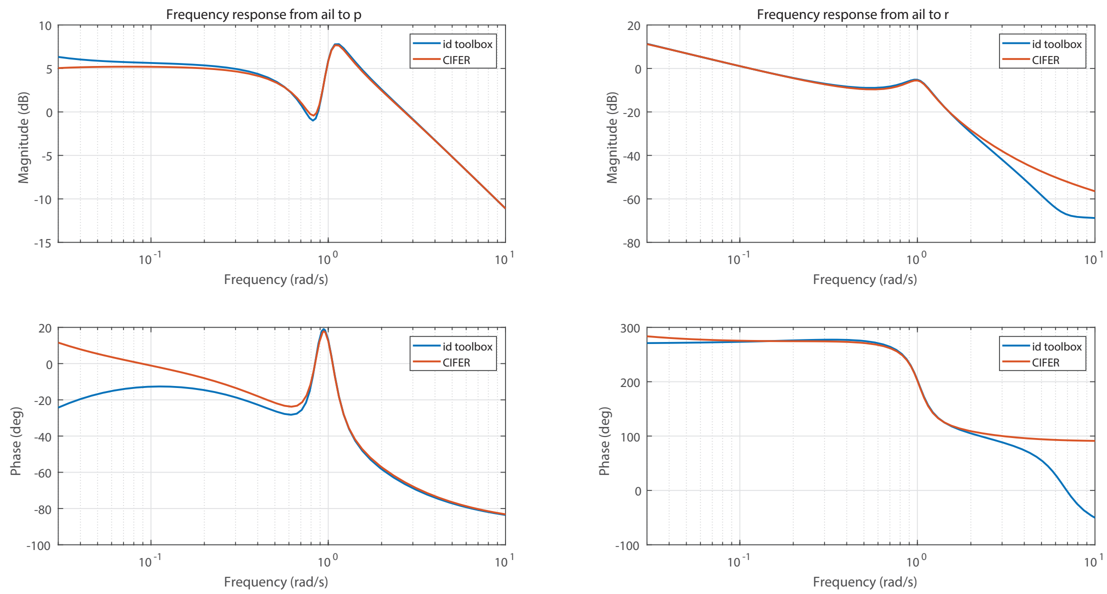

(b) p,r

Figure 35: Comparison of MATLAB®/Identification Toolbox® with CIFER® , aileron input

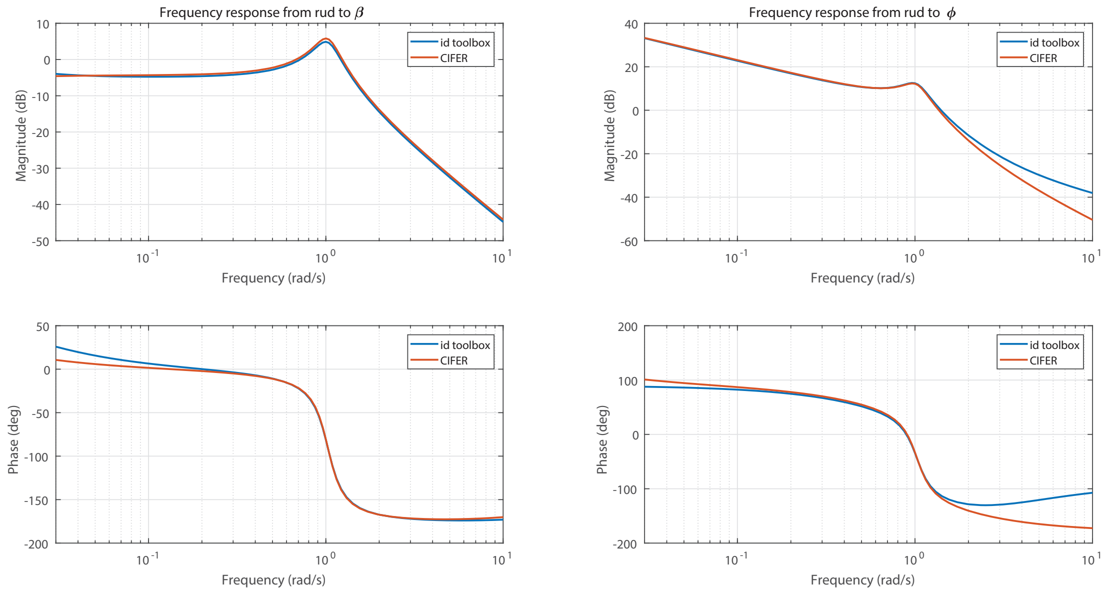

(a) beta,phi

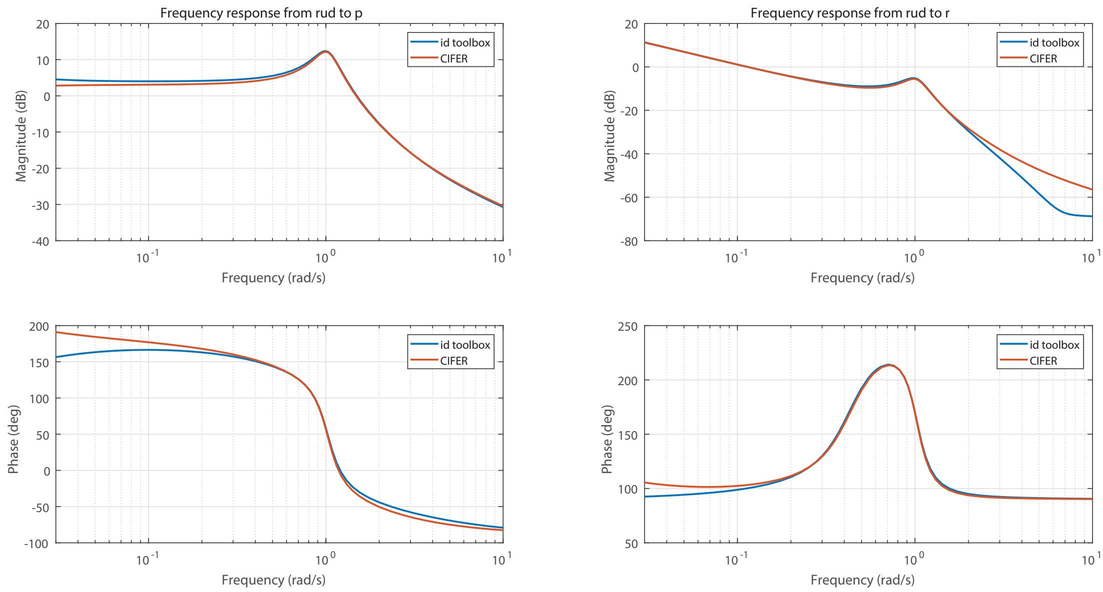

(b) p,r

Figure 36: Comparison of MATLAB®/Identification Toolbox® with CIFER® , rudder input

Finally, figure bellow shows comparison of two identified lateral state-space models using two different methods:
frequency response in CIFER®, and subspace in MATLAB®/Identification Toolbox®.

The figure compares responses to doublet inputs (different inputs than used in excitation) of both models with real-flight of Concorde in FlightGear simulator. Both models give acceptable results in terms of time-responses.

However, being able to identify individual elements of state-matrices with desired structure and accuracy analysis can be required, for example, to properly identify aerodynamic parameters and derivatives of selected aircraft, which seems to be not possible with subspace methods.

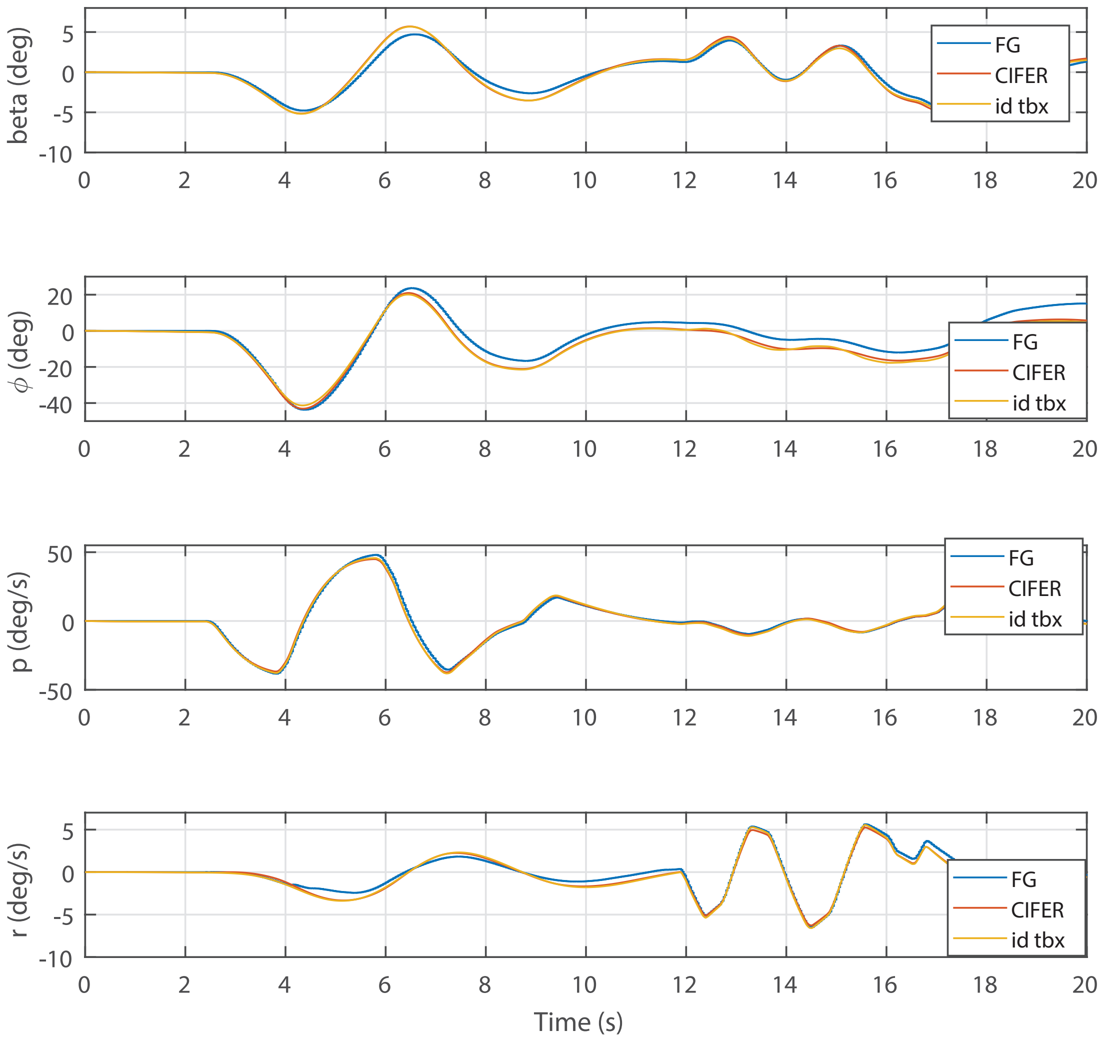

Figure 37: Comparison of flight

10.3 Comparison of computed and identified aerodynamic coefficients

1. Equilibrium
   - airspeed $V_e = 260$ kt $= 133$ m/s
   - angle of attack $\alpha_e = 6.5^\circ = 0.1134$ rad
   - altitude $h = 10\,000$ ft $= 3048$ m
   - air density at h (ISA) $\rho = 0.9$ km/m^3
   - dynamic pressure $\bar{q} = \frac{1}{2}\rho V_e^2 = 8044.06$ Pa
2. Aircraft parameters
   - gross weight $m = 175\,706$ kg
   - mean aerodynamic chord $\bar{c} = 27.66$ m
   - moments of inertia in body axes (as defined in FlightGear for Concorde)
     - $J_X = \frac{m}{10}(R_x \frac{b}{2})^2 = 186\,481{,}587$ kg $\cdot$ m^2, where b is wingspan
     - $J_Y = \frac{m}{10}(R_y \frac{d}{2})^2 = 241\,2358{,}389$ kg $\cdot$ m^2, where d is length
     - $J_Z = \frac{m}{10}(R_z \frac{e}{2})^2 = 127\,0702{,}08$ kg $\cdot$ m^2, where $e = (b+d)/2$

       where $R_x = 0.255$, $R_y = 0.38$, $R_z = 0.39$ for delta wing
   - moments of inertia in stability (wind) axes
     - $J'_x = J_x \cos^2\alpha + J_z \sin^2\alpha - J_{xz}\sin 2\alpha, \quad J_{xz} = 0$
     - $J'_y = J_y$
     - $J'_z = \frac{1}{2}(J_x - J_y)\sin 2\alpha + J_{xz}\cos 2\alpha$
3. Aerodynamic coefficients obtained from FlightGear files
   - Lift-curve slope: $C_{L_\alpha} = 4.4$
   - Pitch damping derivative: $C_{m_q} = -21 \cdot \alpha_{[\text{rad}]}$
   - Pitch stiffness derivative: $C_{m_\alpha} = -0.7 \cdot \alpha_{[\text{rad}]}$
   - Dihedral derivative $C_{l_\beta} = -0.1 \cdot \bar{\beta}_{[\text{rad}]}, \quad \bar{\beta} = 5^\circ = 0.0873$ rad
   - Yaw stiffness derivative $C_{n_\beta} = 0.12 \cdot \bar{\beta}_{[\text{rad}]}$
   - Roll damping derivative $C_{l_p} = -0.4 \cdot \bar{\beta}_{[\text{rad}]}$

Coefficient	Computed value	Identified value	C-R [%]	Insens. [%]
$Z_\alpha = \frac{-\bar{q}S}{m}(C_{D_e} + C_{L_\alpha})$	-72.162	-68.56	6.95	1.41
$M_q = \frac{\bar{q}S\bar{c}}{J_Y}\frac{\bar{c}}{2V_e}C_{m_q}$	-8.139	-8.14	2.92	0.99
$M_\alpha = \frac{\bar{q}S\bar{c}}{J_Y}C_{m_\alpha}$	-2.623	-2.30	8.66	1.67
$L_\beta = \frac{\bar{q}Sb}{J'_x}C_{l_\beta}$	-3.208	-3.26	4.59	1.14
$N_\beta = \frac{\bar{q}Sb}{J'_z}C_{n_\beta}$	0.614	0.66	3.45	0.75
$L_p = \frac{\bar{q}Sb}{J'_x}\frac{b}{2V_e}C_{l_p}$	-1.226	-1.19	12.38	2.70

Table 6: Computed vs identified aerodynamic coefficients

Comparison of selected individual aerodynamic derivatives with values obtained and computed from FlightGear files again proves high quality of achieved identification results, both longitudinal and lateral, with high degree of confidence based on Cramer-Rao and insensitivity.

PART III

MODERN CONTROL SYSTEM DESIGN

11 Introduction

11.1 Limitations of classical control

The essence of classical design is successive loop closure guided by a good deal of intuition and experience that assists in selecting the control system structure. For instance, it is desirable to provide inner rate feedback loops around a plant to reduce the effect of plant parameter variations. In conjunction with this, standard compensator structures are used designed to approximate derivative action to stabilize the system or integral action to eliminate steady-state error.

The one-loop-at-a-time design approach is aided by such tools as root locus, Bode and Nyquist plots, and so on, that enables to visualize how the system dynamics are being modified. However, the design procedure becomes increasingly difficult as more loops are added and does not guarantee success when the dynamics are multi-variable, that is, when there are multiple inputs, multiple outputs, or multiple feedback loops.[3]

11.2 Modern control

Two concepts are central to modern control design. The first is that the design is based directly on the state-variable model, which contains more information about the system than the input-output (black box) description. The state-variable model was introduced into system theory, along with matrix algebra, by R. Kalman.

The second central concept in the expression of performance specifications in terms of a mathematically precise performance criterion which then yields matrix equations for the control gains. Solving matrix equations, in contrast to individual control gains in SISO theory, allows all the control gains to be computed simultaneously so that all loops are closed at the same time.[3]

12 LQR controller theory

Modern techniques are used to design stability and augmentation systems (SAS) and autopilots. This is accomplished by regulating certain states of the aircraft to zero while obtaining desirable closed-loop response characteristics. It involves the problem of stabilizing the aircraft by placing the closed-loop poles at desirable locations.

Instead of computing one-loop-at a time as in classical control, a performance criterion is selected. Once it is selected, the control gains are explicitly computed by matrix design equations, and closed-loop stability will generally be guaranteed, unlike in classical control, where root-locus techniques must be used to pay attention to gain and phase margins.

Different criteria will results in different closed-loop time responses and robustness properties.

Let's assume linear time-invariant state-variable model of the form in equation (9.1), where $\mathbf{x}(t) \in \mathbb{R}^n$ and $\mathbf{u}(t) \in \mathbb{R}^m$. The controls will be output feedback of the form

$$\mathbf{y} = -\mathbf{K}\mathbf{u} \tag{12.1}$$

where $\mathbf{K}$ is an $m \times p$ matrix of constant feedback coefficients to be determined by the design procedure.[3]

12.1 Quadratic performance index

The objective of state regulation for the aircraft is to derive any initial condition error to zero, thus guaranteeing stability. This may be achieved by selecting the control input $u(t)$ to minimize a quadratic cost index or performance index (PI) of the type

$$J = \frac{1}{2}\int_0^\infty \left(\mathbf{x}^T\mathbf{Q}\mathbf{x} + \mathbf{u}^T\mathbf{R}\mathbf{u}\right)\ \mathrm{d}t \tag{12.2}$$

where **Q** and **R** are symmetric positive-semidefinite weighting matrices.

Q is matrix penalizing states - control performance. **R** is symmetric matrix penalizing control action.[3]

12.2 Solution of the LQR problem

Given the linear system (9.1), find the feedback coefficient matrix **K** in the control input (12.1) that minimizes the value of the quadratic performance index (12.2).

By substituting the control (12.1) into (9.1a), the closed-loop system equations are found to be

$$\dot{\mathbf{x}} = (\mathbf{A} - \mathbf{BKC})\mathbf{x} \equiv \mathbf{A_c}\mathbf{x} \tag{12.3}$$

The PI may be expressed in terms of **K** as

$$J = \frac{1}{2}\int_0^\infty \mathbf{x}^T\left(\mathbf{Q} + \mathbf{C}^T\mathbf{K}^T\mathbf{RKC}\right)\mathbf{x}\ \mathrm{d}t \tag{12.4}$$

The design problem is now to select the gain **K** to that J is minimized.[3]

13 Controller design, with integral action

Integral action can be added by augmenting the system with integrators at selected channels to achieve zero steady-state error for constant reference or disturbances.

CAS - control augmentation systems, are designed using MATLAB's *lqr* function.

13.1 Longitudinal CAS

Pitch attitude hold CAS, or autopilot, is designed with integral action to ensure zero steady-state error for step pitch angle θ reference. Simultaneously, the airspeed v is stabilized, hence MIMO controller.

Simple elevator servo and engine delay are also taken into account as actuators, with $\tau_{el} = 0.1s$ and $\tau_{thr} = 2s$.

13.1.1 Augmented system construction

```
Aaug = [A zeros(4,2) B; [0 0 0 1;0 0 1 0] zeros(2,4); [zeros
    (2,6) diag([-0.5, -10])]];
Baug = [zeros(6,2); diag([0.5 10])];
```

13.1.2 Performance index selection

```
Q = diag([1,1,100,.10,1,1,.01,.01]);
R = diag([0.05,.2]);
```

13.1.3 Control gain computation

```
Klong = lqr(Aaug, Baug, Q, R)
```

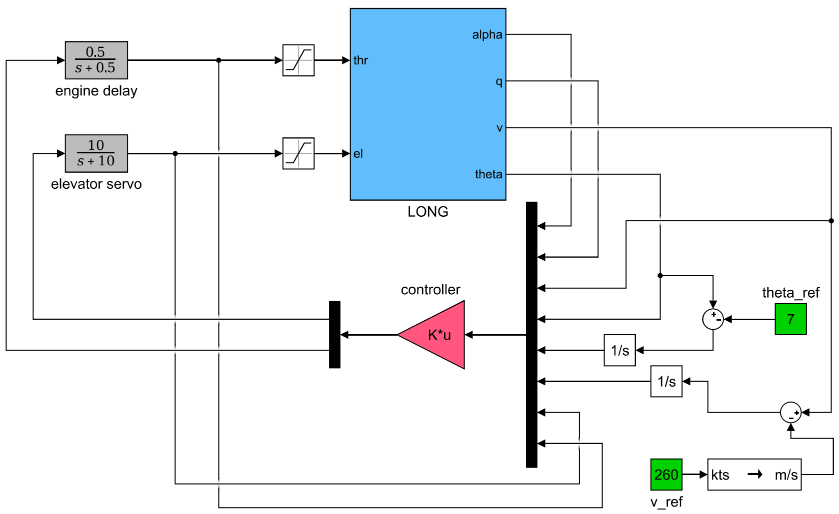

Figure 38: LQR pitch controller with airspeed stabilization

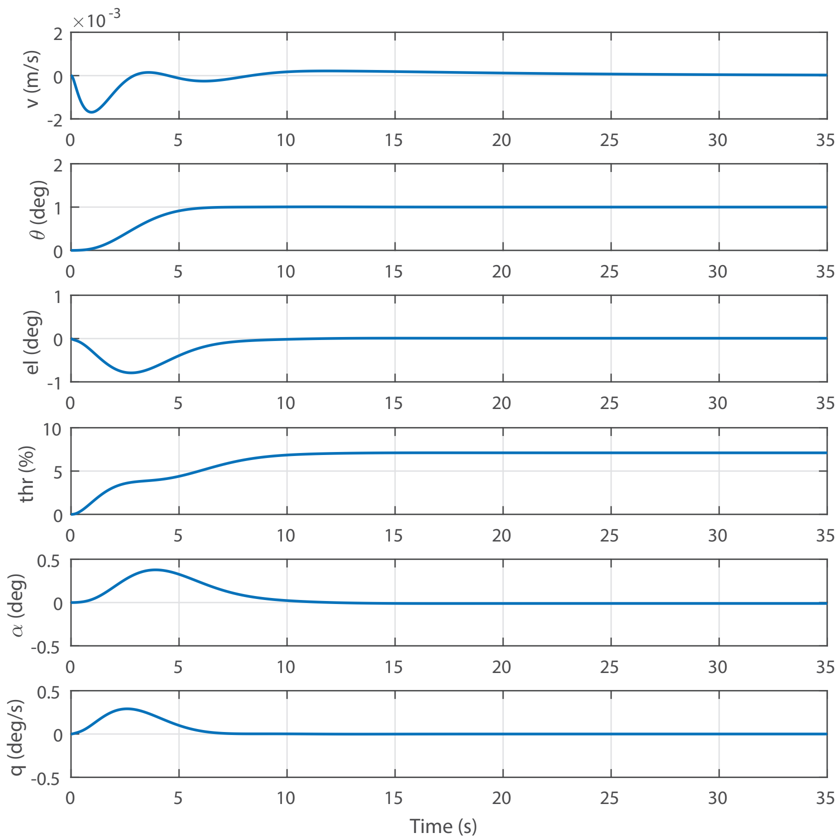

Figure 39: Longitudinal CAS response to reference

13.2 Lateral CAS

Roll-angle (bank) CAS, or autopilot, is designed with integrated yaw-damper and side-slip angle (β) stabilization. Integral action is on β to ensure coordinated turn ($\beta \to 0$).

Aileron and rudder servos are not considered for design, but are validated by simulation and are the same as elevator servo ($\tau_{ail} = \tau_{rud} = 0.1s$).

13.2.1 Augmented system construction

```
Aaug = [A zeros(4,1); 1 0 0 0 0];
Baug = [B; 0 0];
```

13.2.2 Performance index selection

```
Q = diag([50 1 1 1 2]);
R = diag([1 1]);
```

13.2.3 Control gain computation

```
Klong = lqr(Aaug, Baug, Q, R)
```

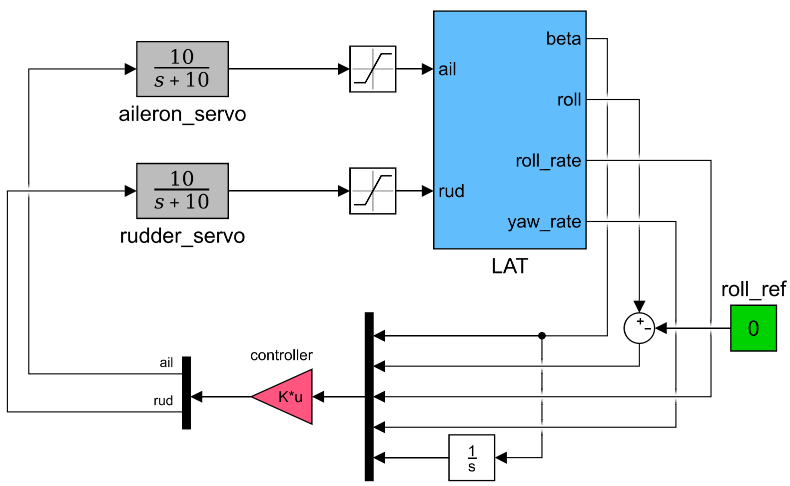

Figure 40: LQR roll-angle controller with β stabilization

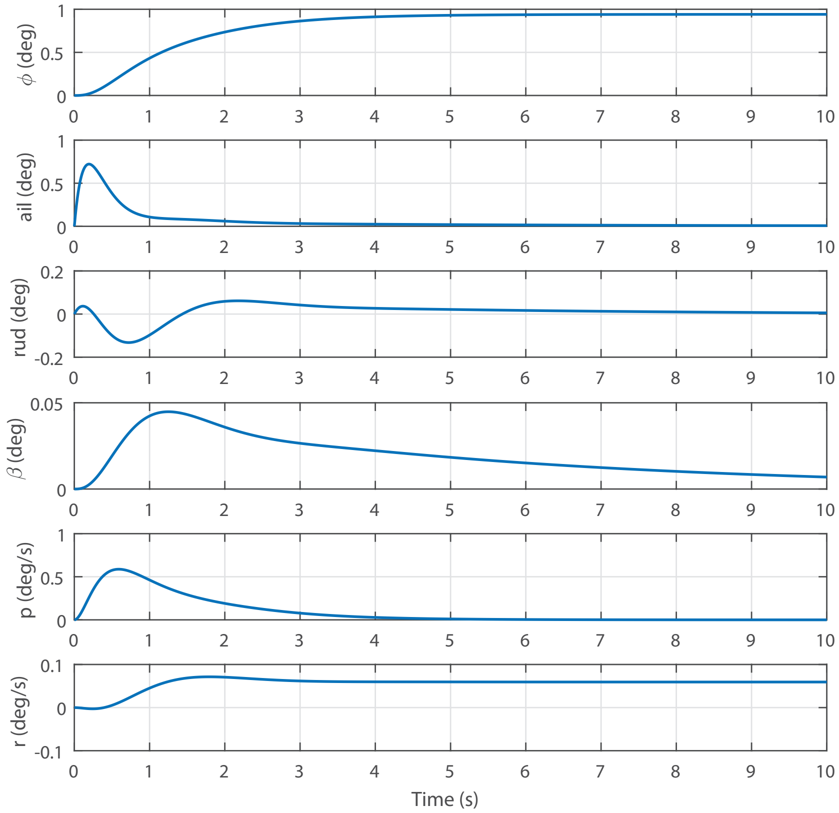

Figure 41: Lateral CAS response to reference

14 Results validation

Figures 42 and 43 show actual test flights performed by Concorde aircraft in FlightGear simulator and controlled by MATLAB®/Simulink®. It's clear that both longitudinal and lateral augmented models follow desired references, pitch-angle, and roll-angle respectively.

The designed CAS systems can be used as basis for another stage of control systems, namely altitude and heading hold, or path following and ILS landing systems.

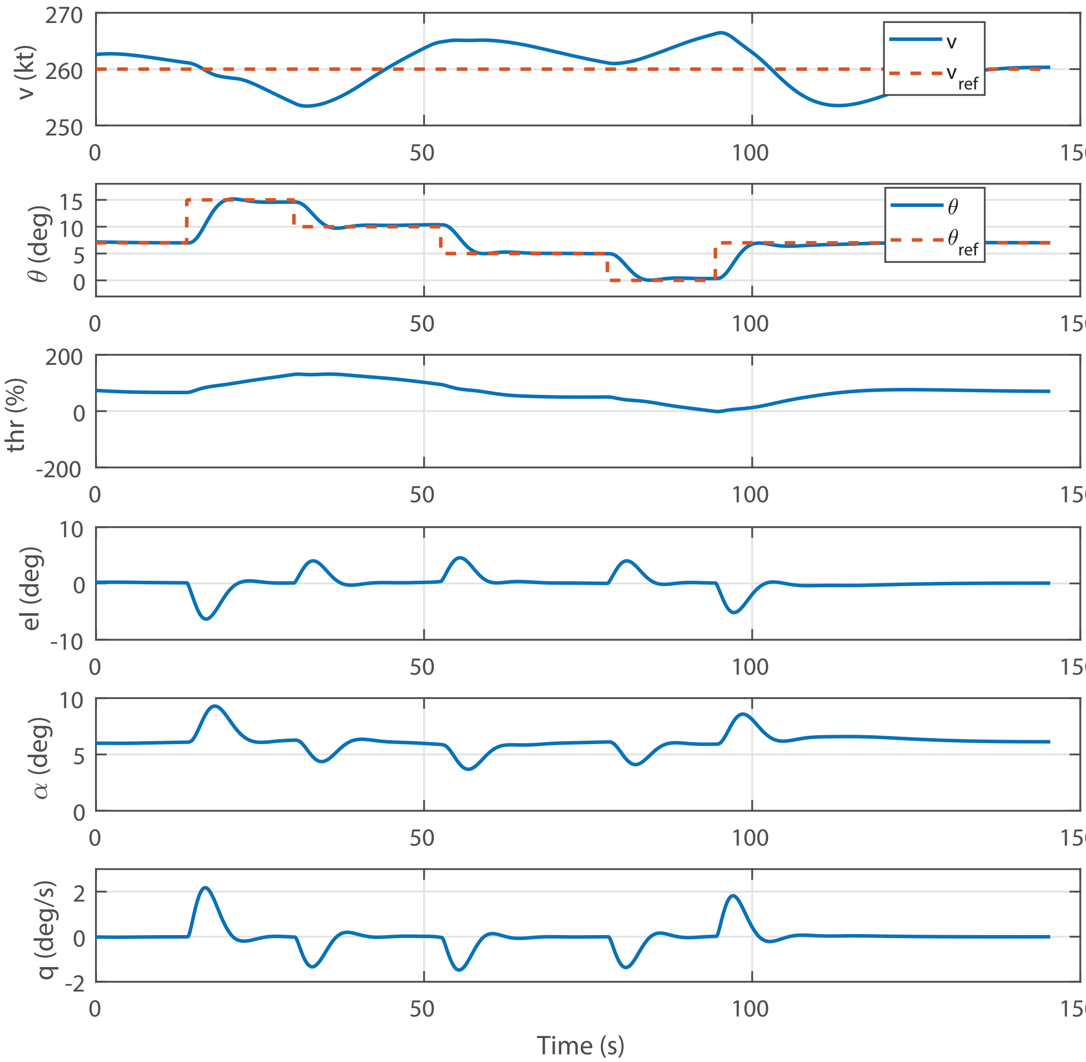

Figure 42: Longitudinal control test flight

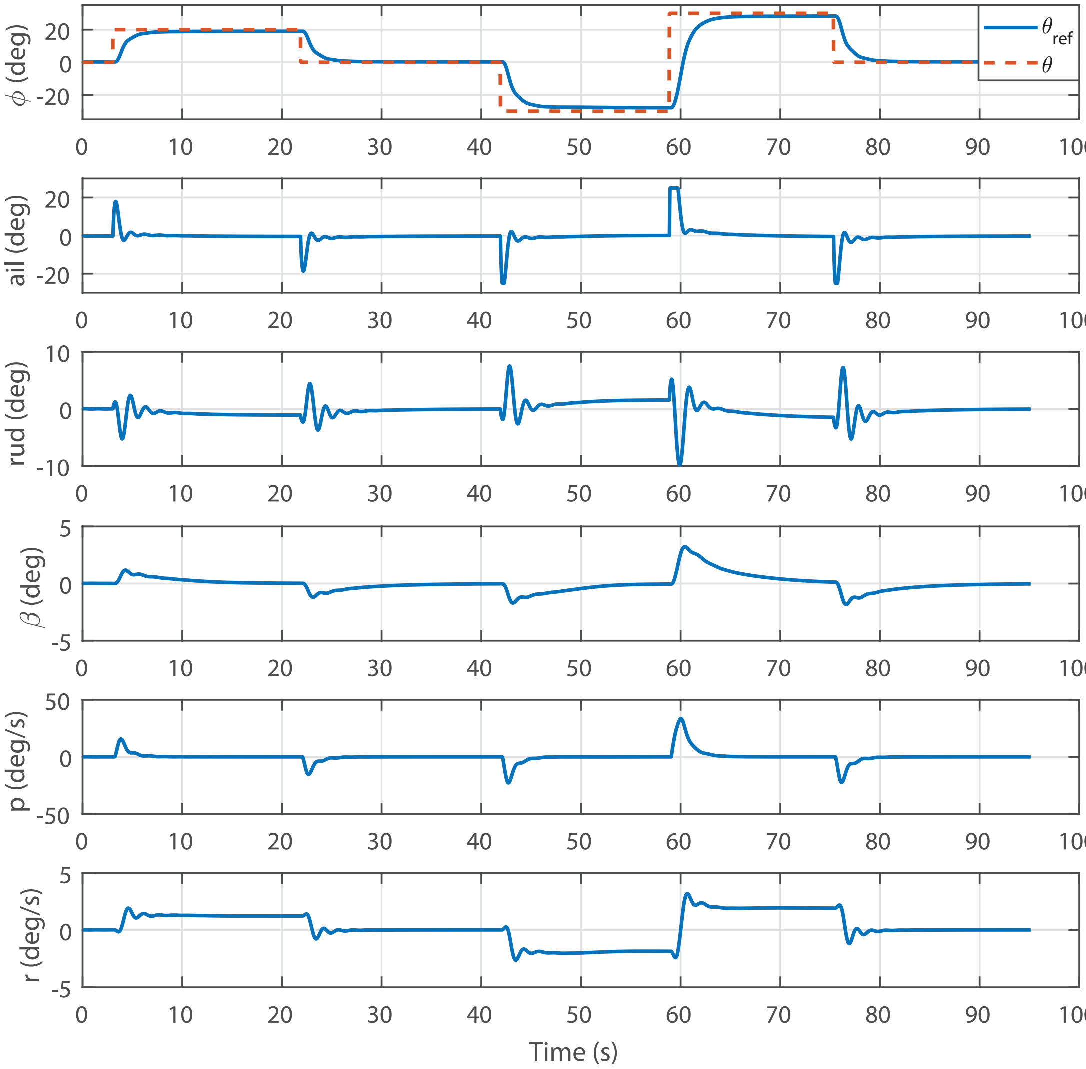

Figure 43: Lateral control test flight

15 Conclusion and further work

The thesis evaluated methods of flight dynamics model identification using frequency response data, which was basis for the followed control system design of simulated aircraft.

First, the interconnection between MATLAB®/Simulink® and high fidelity simulator FlightGear was implemented. This allowed the real-time flight data acquisition of selected aircraft, that was later used for flight dynamics model identification.

The identification itself was performed in software called CIFER®, which exploits latest advancements in dynamics model identification, particularly of aircraft and rotorcraft, using frequency response data. The algorithms implemented and evaluated in this software provide not only great control mechanisms of step-by-step identification process with every subresult being analyzed and improved if necessary, but also high quality of final results. This is the main advantage when compared to traditional time-domain subspace methods, which are utilized for example in MATLAB®/Identification Toolbox®.

The other main advantage of frequency response methods is structured state-space identification, which allows state-space matrices to be identified with desired structure, for example known constants and other parameters. This provides greater physical insight into the model being identified, since each aerodynamic derivative and other parameters can be separately identified and its accuracy analyzed. The comparison of selected individual aerodynamic parameters with values computed from data inside FlightGear proved the high accuracy of identified models. Results from CIFER®were also compared with results of MATLAB®/Identification Toolbox®.

Dynamics models identified using CIFER® software were later used for control system design and implementation. The thesis presented one of the modern MIMO methods of flight control design, Linear Quadratic Regulator, which uses state-space model instead of traditional SISO functions.

Using MIMO LQR regulators not only simplifies the design process, where one-loop-at-a-time approach is replaced with performance index selection, but also allows to achieve better transient responses with guaranteed stability margins.

The final solution was tested in already mentioned high fidelity simulator and test flights again proved high quality of achieved results. Even better results could be achieved with even more advanced flight control systems design methods, e.g. model predictive controller, dynamic inversion etc. where full flight envelope of aircraft could be explored.

The presented process of aircraft dynamics model identification followed by it's control system design and implementation using flight simulator can be used for example as environment for rapid prototyping. Using other high fidelity simulators available, like for example X-Plane® by Laminar Research, which computes aerodynamics of 3D model in real-time during flight, instead of a-priori known look-up tables like FlightGear, could be very useful for fast and cheap control system design of a small UAVs. All it takes is to model the UAV in 3D, put it into X-Plane®, and perform the identification and control system design as described in this thesis. This process could produce a prototype that is ready to fly in real life, or basis for further enhancements.

References

[1] Tischler, Mark B., and Remple, Robert K. *Aircraft and rotorcraft system identification : engineering methods with flight test examples.* Reston, VA: American Institute of Aeronautics and Astronautics, 2012. Print

[2] Tischler, Mark B., and Remple, Robert K. *Aircraft and rotorcraft system identification: engineering methods with flight test examples. Solutions manual* Reston, VA: American Institute of Aeronautics and Astronautics, 2012. Print

[3] Stevens, Brian L., Frank L. Lewis, and Eric N. Johnson. *Aircraft control and simulation : dynamics, controls design, and autonomous systems, 3rd edition.* Hoboken, New Jersey: Wiley, 2015. Print.

[4] Durham, Wayne. *Aircraft flight dynamics and control*. Chichester, West Sussex: John Wiley & Sons, Inc., 2013. Print.

[5] CIFER® user manual

[6] Anderson, John David. *Fundamentals of aerodynamics*. New York: McGraw-Hill, 2011. Print.

[7] Zipfel, Peter H. *Modeling and Simulation of Aerospace Vehicle Dynamics* (2nd Edition). Reston, VA: American Institute of Aeronautics and Astronautics, 2007. Print.

[8] Allerton, David. *Principles of flight simulation*. Chichester: Wiley, 2010. Print.

[9] Etkin, Bernard, and Lloyd Duff. Reid. *Dynamics of flight: stability and control*. Chichester: Wiley, 1996. Print.

[10] Anderson, Brian D. O., and John Barratt. Moore. *Optimal control: linear quadratic methods*. Englewood Cliffs: Prentice Hall, 1990. Print.

[11] Frederick A. Johnsen, *Sweeping forward*, NASA aeronautical book series, 2013, free ebook from www.nasa.gov/ebooks